AD-A225 495

DTIC FILE COPY

Linear and Nonlinear Optical Properties of Small Silicon Clusters

by

Tapio T. Rantala, Mark I. Stockman, Daniel A. Jelski and Thomas F. George

Prepared for Publication

in

Journal of Chemical Physics

DTIC
ELECTE
AUG 21 1990
D

Departments of Chemistry and Physics
State University of New York at Buffalo
Buffalo, New York 14260

August 1990

90 08 20 023

REPORT DOCUMENTATION PAGE

Form Approved
OMB No. 0704-0188

1a. REPORT SECURITY CLASSIFICATION Unclassified	1b. RESTRICTIVE MARKINGS
2a. SECURITY CLASSIFICATION AUTHORITY	3. DISTRIBUTION/AVAILABILITY OF REPORT Approved for public release; distribution unlimited
2b. DECLASSIFICATION/DOWNGRADING SCHEDULE	

4. PERFORMING ORGANIZATION REPORT NUMBER(S) UBUFFALO/DC/90/TR-20	5. MONITORING ORGANIZATION REPORT NUMBER(S)

6a. NAME OF PERFORMING ORGANIZATION Depts. Chemistry & Physics State University of New York	6b. OFFICE SYMBOL (If applicable)	7a. NAME OF MONITORING ORGANIZATION

6c. ADDRESS (City, State, and ZIP Code) Fronczak Hall, Amherst Campus Buffalo, New York 14260	7b. ADDRESS (City, State, and ZIP Code) Chemistry Program 800 N. Quincy Street Arlington, Virginia 22217

8a. NAME OF FUNDING/SPONSORING ORGANIZATION Office of Naval Research	8b. OFFICE SYMBOL (If applicable)	9. PROCUREMENT INSTRUMENT IDENTIFICATION NUMBER Grant N00014-90-J-1193

8c. ADDRESS (City, State, and ZIP Code)
Chemistry Program
800 N. Quincy Street
Arlington, Virginia 22217

10. SOURCE OF FUNDING NUMBERS

PROGRAM ELEMENT NO.	PROJECT NO.	TASK NO.	WORK UNIT ACCESSION NO.

11. TITLE (Include Security Classification)

Linear and Nonlinear Optical Properties of Small Silicon Clusters

12. PERSONAL AUTHOR(S) Tapio T. Rantala, Mark I. Stockman, Daniel A. Jelski and Thomas F. George

13a. TYPE OF REPORT	13b. TIME COVERED FROM _____ TO _____	14. DATE OF REPORT (Year, Month, Day) August 1990	15. PAGE COUNT 51

16. SUPPLEMENTARY NOTATION

Prepared for publication in The Journal of Chemical Physics

17. COSATI CODES			18. SUBJECT TERMS (Continue on reverse if necessary and identify by block number)
FIELD	GROUP	SUB-GROUP	SMALL SILICON CLUSTERS, TIGHT-BINDING MODEL
			OPTICAL PROPERTIES ONE-ELECTRON DENSITY MATRIX
			LINEAR AND NONLINEAR HYPERPOLARIZABILITY.

19. ABSTRACT (Continue on reverse if necessary and identify by block number)
Electronic contributions to the optical properties of small silicon clusters are examined. Geometries and the electronic structures of the clusters are established using the tight-binding model, and linear as well as nonlinear polarizabilities of clusters are evaluated using one-electron density matrix techniques. Kleinman's conjecture for hyperpolarizabilities is shown to be violated in the frequency-degenerate case, which is of practical importance. The nonlinear polarizabilities are found to depend primarily on the symmetry of the cluster and prove to be high for the low symmetry clusters. Possible experiments and applications are discussed.

20. DISTRIBUTION/AVAILABILITY OF ABSTRACT ☒ UNCLASSIFIED/UNLIMITED ☒ SAME AS RPT. ☐ DTIC USERS	21. ABSTRACT SECURITY CLASSIFICATION Unclassified
22a. NAME OF RESPONSIBLE INDIVIDUAL Dr. David L. Nelson	22b. TELEPHONE (Include Area Code) (202) 696-4410	22c. OFFICE SYMBOL

DD Form 1473, JUN 86   Previous editions are obsolete.   SECURITY CLASSIFICATION OF THIS PAGE

LINEAR AND NONLINEAR OPTICAL PROPERTIES
OF SMALL SILICON CLUSTERS

Tapio T. Rantala[†] and Mark I. Stockman[‡]
Departments of Chemistry and Physics & Astronomy
239 Fronczak Hall, State University of New York at Buffalo
Buffalo, New York 14260

Daniel A. Jelski
Department of Chemistry
State University of New York, College at Fredonia
Fredonia, New York 14063

Thomas F. George
Departments of Chemistry and Physics & Astronomy
Center for Electronic and Electro-optic Materials
239 Fronczak Hall, State University of New York at Buffalo
Buffalo, New York 14260

ABSTRACT

Electronic contributions to the optical properties of small silicon clusters are examined. Geometries and the electronic structures of the clusters are established using the tight-binding model, and linear as well as nonlinear polarizabilities of the clusters are evaluated using one-electron density matrix techniques. Kleinman's conjecture for hyperpolarizabilities is shown to be violated in the frequency-degenerate case, which is of practical importance. The nonlinear polarizabilities are found to depend primarily on the symmetry of the cluster and prove to be high for the low-symmetry clusters. Possible experiments and applications are discussed.

[†] Internet address: NSMTAPIO@UBVM.CC.BUFFALO.EDU. Permanent address: Department of Physics, University of Oulu, SF-90570 Oulu, Finland; FYS-TR@FINOU.OULU.FI

[‡] Internet address: NSMARK@UBVMS.CC.BUFFALO.EDU. Also with The Institute of Automation and Electrometry, Siberian Branch of the USSR Academy of Sciences, 630090 Novosibirsk, USSR

1. INTRODUCTION

Small semiconductor clusters in the range from a few atoms to tens of atoms are of a great interest from the viewpoint of both fundamental science[1−5] and applications.[5−8] Their physical properties (symmetry, electronic structure, optical spectra and transition probabilities) differ significantly from those of the solid state both in bulk and at surface, and also from the properties of nanoscale structures, such as quantum dots. Linear and nonlinear optical properties of the latter have been shown to depend strongly on their size in the region of quantum confinement (see, e.g., Refs. 5, 9 and 10). But in these and similar works the bulk electronic structure of the semiconductor is usually assumed and modelled by free electrons with effective mass. Obviously, this approach is valid only for sufficiently large objects with sizes not less than a few nanometers, containing on the order of 1000 atoms or more.

In the present work, for the first time, the optical properties of small silicon clusters with 7 − 13 atoms are predicted. For such clusters, the bulk approximation is not valid and the detailed structure becomes important. Much work has been done on the structure of silicon clusters, both experimentally for stability and photofragmentation[1,2] and for optical absorption,[3,4] and theoretically with *ab initio* type calculations for smaller[11−13] and with other methods for larger[14−19] systems. The approach we use in this paper is based upon the semiempirical tight-binding (TB) model. This model is relatively simple, thus allowing the global optimization of the geometry even for comparatively large clusters. Moreover, the TB model couples the geometry to the electronic structure, which we find essential, but which usually is ignored for larger systems.[14,15] In the previous paper of some of the authors,[17] the TB model was used to find the

2

isomers of Si_{10}, and especially, to trace such subtle effects as Jahn–Teller distortions in geometry. Also, the same method has been succesfully used to reproduce the *ab initio* geometries of other small Si clusters[18,19] and to predict chemical properties of larger clusters.[16] The success of the TB model is due to fitting the parameters of the model to reproduce the band structure of bulk silicon[20], thus establishing a semiempirical basis for reliable calculations of the electronic states.

With the TB geometry and electronic structure and using one-electron density matrix techniques, we obtain closed sum-over-one-electron-states expressions from which linear and nonlinear optical polarizabilities of clusters are subsequently computed. These characteristics govern a number of observable effects: light scattering and absorption by clusters, second harmonic generation, optical rectification, birefringence induced by optical fields and the Kerr effect, phase conjugation, nonlinear corrections to the refraction index, etc.

We show that the nonlinear optical response of a cluster depends mainly on its symmetry and only secondarily on its size, and for low-symmetry clusters the optical nonlinearities prove to be rather high. We attribute such enhancement to a pronounced optical rectification effect.

Small clusters are promising for various applications. The "surface-to-bulk" ratio is extremely large for such clusters, which should imply their increased chemical reactivity, and catalytic and photocatalytic efficiency. Also, the clusters may find numerous applications as materials for nonlinear optics, including optical information processing, provided one is able to accumulate them in some matrices like zeolites, which form

3

large (on the molecular scale) cages.[8] The optical applications of the clusters are based upon their enhanced optical hyperpolarizabilities. Due to small sizes of the clusters. the response times of the optical nonlinearities are expected to be very short. probably on the femtosecond scale.

The next section contains a description of the TB method and the derivation of closed expressions for optical responses with the use of one-electron density matrix techniques. In Sec. 3 the numerical results for these responses are given. Section 4 contains discussion of the obtained results and underlying physical principles. and also suggestions for possible experiments.

4

2. THEORY

The semiempirical tight-binding (TB) model that we use is based on a model Hamiltonian including only nearest-neighbor interactions between the atoms in the cluster and the matrix elements fitted to experimental data. Here, we adopt the model and fit to the bulk Si band structure by Chadi,[20] who used the model for surface studies. We also include the extensions by Tománek and Schlüter[18] to incorporate the detailed interatomic repulsions and coordination dependency in the cohesion of small clusters.

We write the TB Hamiltonian as

$$H_{TB} = \sum_{\mu a} \varepsilon_a^0 \, a_{\mu a}^\dagger a_{\mu a} + \sum_{\mu a\, \nu b} V_{\mu a\, \nu b}\, a_{\mu a}^\dagger a_{\nu b} \ , \tag{1}$$

where $a_{\mu a}^\dagger$ and $a_{\mu a}$ are electron creation and annihilation operators in the basis $|\mu a\rangle = \varphi_a(\mathbf{r} - \mathbf{R}_\mu)$, with $\varphi_a = \{3s, 3p_x, 3p_y, 3p_z\}$ as the valence orbitals of silicon atom at the sites μ with coordinates $\mathbf{R}_\mu$. The basis $|\mu a\rangle$ is not strictly orthonormal, but we neglect the intersite overlap for all operators except the Hamiltonian. In particular, we write the overlap matrix as

$$\langle \nu b|\mu a\rangle = \delta_{\nu\mu}\delta_{ba} \tag{2}$$

in the diagonalization procedure. This is usually called the orthogonal TB.

To reproduce the bulk silicon band structure with the nearest-neighbor distance 2.35 Å, the diagonal matrix elements of the Hamiltonian (1) were fitted[20] to the values ε_s^0 = –5.25 eV and ε_p^0 = 1.20 eV, and the off-diagonal elements to $V_{ss\sigma}$ = –1.938 eV, $V_{sp\sigma}$ = 1.745 eV, $V_{pp\sigma}$ = 3.050 eV and $V_{pp\pi}$ = –1.075 eV. The off-diagonal matrix elements were taken to behave Slater–Koster–like[21] in their angle and distance dependence, and

so their bond length dependence is $1/r^2$ until 3.3 Å. where we consider the bond to be broken.[17]

The diagonalization of the Hamiltonian gives the one-electron energies ε_p and the eigenvectors C_p. Thus, we can write the one-electron states of the occupied and unoccupied valence levels as

$$|p\rangle = \sum_{\mu a} C_{p\mu a} |\mu a\rangle \quad , \tag{3}$$

and the cohesion energy of the N atoms due to the bond formation, which we call the "band structure" energy, can be written as

$$E_{BS} = \sum_p n_p \varepsilon_p - N \sum_a n_a^0 \varepsilon_a^0 + U \sum_\mu (q_\mu - q_\mu^0)^2 \quad , \tag{4}$$

where n_p and n_a^0 are occupation numbers, and the difference between the two first terms is the stabilization energy of the four free-atom valence levels ε_a^0 due to the bonding. The third term in Eq. (4) is added to include the intra-atomic Coulomb repulsion caused by charge transfer within the cluster, and it is evaluated using the Mulliken charges q_μ and q_μ^0, with the constant U taken to be 1 eV.[18]

A repulsion energy term is finally added to account for the structure of small clusters. It is the sum of interatomic pair potentials $E_d(R_{\mu\nu})$ and a term depending on the bond number N_b,

$$E_R = \sum_{\mu < \nu}^N E_d(R_{\mu\nu}) - N\left[c_1\left(\frac{N_b}{N}\right)^2 + c_2\left(\frac{N_b}{N}\right) + c_3\right] \quad . \tag{5}$$

This term has been fitted[18] within the present TB model to reproduce the bulk cohesion energies 4.64 eV and 4.24 eV for the diamond and FCC structures, respectively, and the *ab initio* potential curve of the silicon dimer. This leads to constants $c_1 = 0.225$

eV. $c_2 = 1.945$ eV and $c_3 = -1.03$ eV. which therefore set the second term to zero for Si_2. Finally, the total cohesion energy of the cluster is written as a sum of the band structure energy E_{BS} and the repulsion energy E_R,

$$E_{coh} = -(E_{BS} - E_R) \ ,$$ (6)

which is maximized to find the structures of the Si clusters in the present work.

The orthonormality approximation (2) is usually adopted to also derive the matrix elements of multipole operators (see, e.g., Ref. 22). Then the dipole transition matrix elements $(\mathbf{r})_{pq}$, which we need to evaluate the optical properties. can be written as

$$(\mathbf{r})_{pq} = \sum_{\mu a} C^*_{q\mu a} C_{p\mu a} \mathbf{R}_\mu + \sum_{\mu ab} C^*_{q\mu b} C_{p\mu a} (\mathbf{r})_{ab} \ ,$$ (7)

where the atomic transition matrix elements are

$$(\mathbf{r})_{ab} = \int \varphi^*_b(\mathbf{r}) \ \mathbf{r} \ \varphi_a(\mathbf{r}) \ d\mathbf{r} \ .$$ (8)

The first term in Eq. (7) is Mulliken-like and diagonal in the atomic basis, and it can be evaluated directly from the TB eigenvectors and nuclear coordinates $\mathbf{R}_\mu$. In the system of noninteracting atoms, this term vanishes and the second term gives the sum of the atomic displacement polarizations, which is proportional to the size of the system. In the Appendix we show that the first term is nonzero only when the atomic wavefunctions overlap and delocalized molecular one-electron states are formed. Hence, the first term in (7) is identified to give the charge transfer or molecular displacement polarization contribution to the transition matrix element.

7

The second term, on the other hand, involves the atomic transition matrix elements (8) $(r_i)_{ba} = \langle 3p_x|x|3s\rangle = \langle 3p_y|y|3s\rangle = \langle 3p_z|z|3s\rangle$ for silicon. We estimated these to be about 0.66 Å using the Slater type Si $3s$ and $3p$ orbitals with the effective core charge 4.15 e.[23] This value has been adopted for our numerical calculations. The value found from the experimental data[24] on the transition oscillator strengths for Si III is 0.46 Å, in which case the Slater orbitals give 0.57 Å, thus verifying our estimate to be reasonable.

The relative importance of these two terms depends on the nature of the system, i.e., the detailed electronic structure. Usually (see, e.g., Ref. 22), the strong nonlinear optical response of polymers is interpreted in terms of the molecular displacement polarization through delocalized π electrons without a quantitative justification. However, this interpretation may not be always so obvious, especially in the case of small semiconductor clusters. We carried out numerical calculations which showed that when the second term in Eq. (7) is neglected, the linear optical responses decrease typically by 20 percent, while nonlinear polarizabilities in some cases become several times smaller. We verified that it is the interference of the two terms considered that gives the major contribution to hyperpolarizabilities in many cases.

To find the optical responses of the clusters, we use density matrix techniques. However, rather than the conventional many-electron matrix,[26,27] we employ the one-electron density matrix, which exactly takes into account the Fermi statistics of electrons. The one-electron density matrix is defined as $\rho_{pq} = \langle a_q^\dagger a_p\rangle$, where $a_q^\dagger$ and a_p are the Fermi creation and annihilation operators in the one-electron states $|q\rangle$ and $|p\rangle$, respectively, and $\langle ...\rangle$ denotes quantum-mechanical (and statistical) average over the

8

state of the cluster.

The Hamiltonian of the electrons is now

$$H = \sum_p \varepsilon_p a_p^+ a_p - \sum_{pq} V_{pq}(t) a_p^\dagger a_q \ , \tag{9}$$

where the matrix element of the interaction between an electron and the electromagnetic field has the form

$$V_{pq}(t) = -e \sum_\omega (\mathbf{r})_{pq} \mathbf{E}(\omega) e^{-i\omega t} \ . \tag{10}$$

the the matrix element $(\mathbf{r})_{pq}$ is given by Eq. (7), and $\mathbf{E}(\omega)$ is the electric field of the exciting wave at the frequency ω and $\mathbf{E}^*(\omega) = \mathbf{E}(-\omega)$.

The equation of motion for ρ_{pq} can readily be obtained by commutation of $a_q^\dagger a_p$ with the Hamiltonian using the Fermi anticommutation relations between the operators $a^\dagger$ and a as

$$i\hbar \frac{\partial \rho}{\partial t} = [\varepsilon + V(t), \rho] - i\hbar [\Gamma, \rho]_+ \ , \tag{11}$$

where the energy ε, relaxation matrix Γ and interaction V are operators in the space of the one-electron states, Γ is supposed to be diagonalized together with ε, and $[\ ]_+$ denotes the anticommutator.

The differential operator equation (11) can be transformed into the equivalent integral matrix equation

$$\rho_{pq}(t) = i \int_{-\infty}^{t} e^{i(\varepsilon_{pq} - i\Gamma_{pq})(t'-t)} [\rho(t'), V(t')]_{pq} \, dt' \ . \tag{12}$$

The iterative solution of this equation generates a perturbation series for ρ of the usual type. To start with, the zeroth-order solution is diagonal. $\rho_{pq}^{(0)} = \delta_{pq} \rho_p^{(0)}$, where $\rho_p^{(0)} =$

$\theta(\varepsilon_F - \varepsilon_p)$ is the Fermi population factor and ε_F is the Fermi-level. The nth-order contribution to the density matrix has the form

$$\rho^{(n)}_{i_1\ldots i_n}(\omega_1, \omega_2, \ldots, \omega_n) \exp\left\{-it\sum_{k=1}^{n}\omega_k\right\} E_{1i_1}E_{2i_2}\ldots E_{ni_n} \ . \tag{13}$$

where ω_k and E_{ki_k} are frequencies and amplitudes of the contributing fields, with summation over recurrent vector indices implied. The positive frequency corresponds to absorption of photons and negative to emission. The nth-order polarizability is
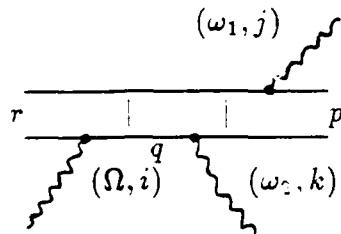
$$\alpha^{(n)}_{ii_1\ldots i_n}(\Omega; \omega_1, \ldots, \omega_n) = e \ \text{Tr}\{\rho^{(n)}_{ii_1\ldots i_n}(\omega_1, \ldots, \omega_n)r_i\} -$$
$$- \text{permutations of all pairs } (\omega_1, i_1), \ldots, (\omega_n, i_n) \ . \tag{14}$$

with the resulting (generated) frequency $\Omega = -\sum_{k=1}^{n}\omega_k$.

The perturbation series for $\alpha^{(n)}$ is conveniently represented by means of double Feynman diagrams. For example, one of the second-order contributions to $\alpha^{(2)}$ is given by

$$= e^2 \sum_{pqr} \frac{(r_k)_{pr}(r_i)_{rq}(r_j)_{qp}}{(-\Omega - \omega_{qr} + i\Gamma_{qr})(\omega_1 - \omega_{pr} + i\Gamma_{pr})}\rho^{(0)}_p \ . \tag{15}$$

Here one can trace the diagrammatic rules. Horizontal lines correspond to one-electron states over which summation is implied. These lines are separated by vertices, and the vertex between the lower p and q lines corresponds to $-e(\mathbf{r})_{qp}$, and between the upper r and p lines to $e(\mathbf{r})_{pr}$. The vertical lines connecting the states r and q denote one-electron propagators $[\sum \omega_k - \omega_{qr} + i\Gamma_{qr}]^{-1}$, where $\sum \omega_k$ is the sum of all photon frequencies to

10

the right of the propagator. $\omega_{qr} = (\varepsilon_q - \varepsilon_r)/\hbar$ is the transition frequency between the one-electron states. and the free p lines denote $\rho_p^{(0)}$. A pass along the diagram goes from right to left along the lower line and back to the right along the upper line. The present diagrammatic technique is similar to the conventional one.[26,27] with the difference that here all the operators and states are one-electron ones. Contributions of all many-electron states, which appear in the many-electron techniques. either reduce to those of one-electron states or cancel due to the Fermi statistics of electrons.

The (hyper)polarizability tensor $\alpha^{(n)}_{ii_1\ldots i_n}(\Omega;\omega_1,\ldots,\omega_n)$ is the sum of all different n^{th}-order diagrams, including the permutations of photons. As an example. we give the explicit expression for the second-order polarizability,

$$
\alpha^{(2)}_{ijk}(\Omega;\omega_1,\omega_2) =
$$
$$
= -\sum_{pqr}\rho_p^{(0)}\left\{ \frac{(r_i)_{pr}(r_j)_{rq}(r_k)_{qp}}{(-\Omega - \omega_{rp} + i\Gamma_{rp})(\omega_2 - \omega_{qp} + i\Gamma_{qp})} + \frac{(r_i)_{pr}(r_k)_{rq}(r_j)_{qp}}{(-\Omega - \omega_{rp} + i\Gamma_{rp})(\omega_1 - \omega_{qp} + i\Gamma_{qp})} \right.
$$
$$
+ \frac{(r_k)_{pr}(r_j)_{rq}(r_i)_{qp}}{(-\Omega + \omega_{qp} + i\Gamma_{qp})(\omega_2 + \omega_{rp} + i\Gamma_{rp})} + \frac{(r_j)_{pr}(r_k)_{rq}(r_i)_{qp}}{(-\Omega + \omega_{qp} + i\Gamma_{qp})(\omega_1 - \omega_{rp} + i\Gamma_{rp})}
$$
$$
- \left(\frac{(r_k)_{pr}(r_i)_{rq}(r_j)_{qp}}{(\omega_2 + \omega_{rp} + i\Gamma_{rp})(\omega_1 - \omega_{qp} + i\Gamma_{qp})} + \frac{(r_j)_{pr}(r_i)_{rq}(r_k)_{qp}}{(\omega_1 + \omega_{rp} + i\Gamma_{rp})(\omega_2 - \omega_{qp} + i\Gamma_{qp})} \right)
$$
$$
\left. \times \left(1 + \frac{2i\Gamma_p}{-\Omega - \omega_{qr} + i\Gamma_{qr}} \right) \right\} ,
$$

$$(16)$$

where $\Omega = -(\omega_1 + \omega_2)$. The third-order polarizability is given by 48 diagrams. The different diagrams were written in the computer code in the form of the permutations of one basic diagram relevant to the order n. The CPU time on VAX 6420 for computation of one component of the third-order polarizability is on the order of an hour depending on the cluster size, whereas it is only minutes and seconds for the second- and first-order

11

cases. respectively. This increase in the CPU time is due to the multiple sum over all (occupied and unoccupied) one-electron levels.

The (hyper)polarizability tensor $\alpha_{ii_1...i_n}^{(n)}(\Omega;\omega_1,\ldots,\omega_n)$ has trivial permutation symmetry: all frequencies, except for the frequency of the resulting field, can be permuted together with the corresponding polarization indices. Kleinman's conjecture[28] states that the permutation symmetry is also valid for (Ω,i) of the resulting field. This conjecture allows one to greatly reduce the number of independent elements of the polarizability tensor $\alpha_{ii_1...i_n}^{(n)}$ in the the degenerate cases when the resulting frequency Ω coincides with some of the exciting frequencies ω_k. In particular, the static polarizability $\alpha_{ii_1...i_n}^{(n)}(0,0...,0)$ should be a completely symmetric tensor over all the indices $i, i_1, ..., i_n$. We show here, however, that Kleinman's conjecture does not hold in degenerate cases, particularly, if any of the exciting frequencies ω_i, or the sum of any of these frequencies, is zero or much less in modulus than the relaxation rates Γ. This conclusion is confirmed by the numerical results in Sec. 3. The violation of Kleinman's conjecture has, to the best of our knowledge, never been noticed before in the literature.

Let us start from the second-order polarizability (16). Usually, Kleinman's conjecture is proven[26] by assuming that none of the frequencies ω_k or their sums coincide with any of the transition frequencies ω_{pq}. In this case, the small relaxation constants Γ in (16) could be neglected, and the resulting expression explicitly obeys Kleinman's symmetry. The reason why Kleinman's conjecture fails is very simple and of general validity. In the case of the second-order polarizability, the system should be noncentrosymmetric. As a result, there are always matrix elements $(r)_{pq}$ between the states p and q with identical energies. In particular, there exist diagonal matrix elements $(r)_{pp}$. Apart from

the latter. the coordinate operator r also connects states which are time-reversed with respect to each other and. consequently. have coinciding energies in the absence of an external magnetic field in accord with Kramers's theorem. Such states belong to two-dimensional representations (E) of the point group of the system. Hence. in Eq. (16) there are always propagators whose real parts become small if any of the frequencies Ω, ω_1, and ω_2 are small compared to Γ. Therefore, one cannot neglect the relaxation constants Γ, and the expression (16) is not symmetric with respect to permutation of (Ω, i) with $(\omega_1. j)$ or (ω_2, k). In particular. the static hyperpolarizability $\alpha^{(2)}_{ijk}(0.0.0)$ is not a completely symmetric tensor.

The asymmetric part of the static polarizability can be easily found from (16) and written as

$$\alpha^{(2)a}_{ijk} = \sum_{pq}' \frac{\rho_p}{\omega_{qp}^2} \left[\frac{2\Gamma_q}{\Gamma_p}(r^k_{p\bar{p}} r^i_{\bar{p}q} r^j_{qp} + r^j_{p\bar{p}} r^i_{\bar{p}q} r^k_{qp}) + \frac{\Gamma_p}{\Gamma_q}(r^k_{p\bar{q}} r^i_{\bar{q}q} r^j_{qp} + r^j_{p\bar{q}} r^i_{\bar{q}q} r^k_{qp}) \right] , \qquad (17)$$

where the index $\bar{p}$ stands for any state coinciding in energy with p, and in the summation $q \neq \bar{p}$. Note that this expression depends only on ratios of the the relaxation constants and not on the constants themselves, hence being regular when $\Gamma_{p,q} \to 0$. It is obvious from (16) that, unlike the static limit, in the quasistatic region, i.e., when $\Gamma \ll |\omega_{1,2}| \ll \varepsilon_F/\hbar$, the relaxation constants can be neglected and Kleinman's conjecture holds.

The higher even-order polarizabilities can be considered in a similar way. It can be shown that for odd-order hyperpolarizabilities. Kleinman's conjecture fails irrespective of the existence of a center of symmetry.

13

3. NUMERICAL RESULTS FOR STRUCTURE AND OPTICAL PROPERTIES OF THE CLUSTERS

We consider various geometries of Si_{10} clusters, as discussed in Ref. 17 and shown in Fig. 1. Of the possible BTA related structures,[17] we include only the most stable form, DBTA-I, which also has the largest band gap. We also include Si_7 and Si_{13} clusters in "pentagonal geometry" as suggested in Refs. 11, 12 and 14, and shown in Fig. 1. The geometries of all these clusters were determined by maximizing the cohesion energy in Eq. (6). The resulting electronic structure data and the corresponding point groups of symmetry are given in Table 1. Note that none of the point groups listed, except I_h, possesses a center of symmetry. The coordinate system with respect to clusters is positioned in such a way that in the cases of the point groups C_{2v}, C_{3v}, and D_{5h}, the z-axis coincides with the rotational axes, and one of the mirror planes coincide with the yz-coordinate plane; for the T_d group, the mirror four-fold axes are parallel to the coordinate axes. Below we shall refer to the clusters considered by simply indicating their point groups. We shall not discuss the spectra of one-electron levels since they were already described in details in Ref. 11.

Let us proceed to the optical (dielectric) properties and consider first the static dipole moments $\mathbf{d}$ of the clusters. For the cases of the D_{5h}, T_d and I_h clusters, $\mathbf{d} = 0$, and for the clusters C_{2v} and C_{3v}, the values d_z are 8.5 and −8.3 D, with other components being zero.

Proceeding to the linear polarizability $\alpha_{ij}(\omega) \equiv \alpha_{ij}^{(1)}(-\omega;\omega)$, the α_{ij} tensor is diagonal in all cases. For the nonresonant conditions, $\mathrm{Re}\alpha$ determines light scattering and

Imα vanishes. The calculated nonzero components of Reα_{ij} are shown in the Table 2. They agree with the rough estimate $\alpha_{ii} \simeq R_0^3 N = 90 \times 10^{-24}$ cm^3 to 170×10^{-24} cm^3 for the clusters considered, where $R_0 \simeq 2.5$ Å is the bond length and N is the number of atoms. This estimate is valid for the nonresonant frequencies, for which $\epsilon - 1 \sim 1$, where ϵ is the dielectric constant of the cluster material.

The absorption cross-sections of the clusters, $\sigma_a = (4\pi/3)k$ Imα_{ii}, where $k = 2\pi/\lambda$ is the wavevector of light, are shown in Fig. 2. To calculate the absorption we had to specify the relaxation constants arbitrarily as $\Gamma = 5 \times 10^{-3}$ eV, which qualitatively corresponds to vibration broadening or relaxation on the order of 10^{13} s^{-1}. In turn, the relative heights of the absorption peaks in Fig. 2 correctly reproduce the distribution of oscillator strengths for the electronic transitions, while the absolute value of the cross-section is only a rough estimate. As one can see from Fig. 2, the optical absorption in the visible and near–UV regions depends strongly on the symmetry of the clusters. The qualitative conclusion is that the higher the symmetry (in the qualitative order $C_{2v} < C_{3v} < D_{5h} < T_d, I_h$), the smaller the number of lines observed in the the absorption spectrum, and the greater line shift toward the UV region. This originates from the fact that in the case of higher symmetry, there exist more selection rules, and fewer transitions are allowed. It is necessary to note, however, that we take into account only purely electronic transitions, and allowing for the phonon–electron coupling would bring about the appearance of electronically-forbidden lines in the spectra. In Sec. 4 we shall suggest experiments to directly measure the absorption cross-section of single clusters.

Let us proceed to the second-order hyperpolarizability, which is usually denoted as

15

$\beta_{ijk}(\omega_1, \omega_2) \equiv \alpha_{ijk}^{(2)}(-(\omega_1 - \omega_2); \omega_1, \omega_2)$. This quantity is known to be highly structure-dependent. For the centrosymmetric I_h clusters, obviously, $\beta = 0$. It can be shown that β vanishes also for the noncentrosymmetric D_{5h} clusters. This is a consequence of two symmetry operations: reflection in the xy-plane ensures that number of z-indices of β_{ijk} should be even; simultaneously, the rotation symmetry around the 5-fold axis forbids tensors in the xy-plane with an odd order $n < 5$. This consideration leads also to selection rules for the third-order polarizability (see below). For the symmetry-allowed cases from (16), one can get an order of magnitude estimate of $\beta \sim \alpha(eL_0/\hbar\Delta\omega)$, where $\Delta\omega$ is the detuning of the exciting radiation from the absorption edge of the cluster, and L_0 is a characteristic length of the charge delocalization. Using $\alpha = 10^{-22}$ cm^3 (cf. Table 2) and $L_0 = R_0 = 2.5 \times 10^{-8}$ cm, $\hbar\Delta\omega = 1$ eV, one gets $\beta \simeq 7 \times 10^{-28}$ esu. This estimate is an upper one, since it is assumed that all the atoms, which give rise to linear polarizability, also contribute to β. Indeed, the centrosymmetric part of the polarizability cancels from β. In fact, the magnitude of $\beta \sim 10^{-27}$ esu is considered high, and is characteristic of organic dyes near the resonant (absorption) edge.[29]

The calculated values of all independent components of β_{ijk} together with the symmetry-determined relations between different components are summarized in Table 3. All of these relations have been confirmed by direct numerical calculations to be correct with error less than one percent with regard to allowed elements, the precision being consistent with the deviation from the exact symmetry of the cluster geometries obtained. The data are given for hyperpolarizabilities $\beta_{ijk}(\omega, \omega)$ and $\beta_{ijk}(-\omega, \omega)$ governing two important physical effects: second-harmonic generation (SHG) and optical rectification.[26] For the sake of brevity, we skip the data for $\beta_{ijk}(0, \omega)$ which determines

16

the Pockels effect. Though Kleinman's conjecture does not hold for degenerate cases (see Sec. 2 and below), with a precision within 30 percent. one can nevertheless estimate $\beta_{ijk}(0,\omega) \approx \beta_{jik}(-\omega,\omega)$.

As we can see from Table 3, the magnitude of β strongly depends on the symmetry: all the clusters listed contain the same number $N = 10$ atoms, but maximum elements of β differ several times, the most symmetric T_d cluster being the least efficient with respect to the second-order nonlinearity. The maximum matrix elements of β are of the order of 10^{-28} to 10^{-27} esu. Thus, the nonlinearity proved to be high.

Let us discuss the dispersion (frequency dependence) of β. First note that there exists an appreciable difference between the static case, $\omega_{1,2} = 0$, and the quasistatic case, $0 < \hbar\omega_{1,2} = 10^{-3}$ eV $\ll \hbar\Gamma$ (see Sec. 2). Thus, the dispersion in the region of the relaxation frequencies, $\omega \simeq \Gamma$, is rather strong (practically, this region can belong to an IR or far-IR band). This fact is due to the existence of the diagonal (in energy) dipole matrix elements and is intimately coupled to a violation of Kleinman's conjecture. Between the relaxation region and electronic absorption region, i.e., for $\hbar\Gamma \ll \hbar\omega \leq 0.5$ eV, the dispersion is rather weak. Strong dispersion corresponds to an interband transition with frequency $\omega_g = \varepsilon_g/\hbar$, where ε_g is the HOMO–LUMO energy gap. In the case of SHG, the long-wave dispersion is due to the two-photon resonance, $\omega \approx \omega_g/2$. The rectification and Pockels effects begin to be strongly dispersive at $\omega \approx \omega_g$ due to the single-photon resonance.

Using Table 3, one can easily trace violation of the Kleinman's conjecture. For the T_d symmetry, Kleinman's conjecture is superceded by the group-symmetry and is therefore

17

valid. But in the case of the C_{2v} and C_{3v} clusters, it yields the nontrivial prediction for $\omega_{1,2} = 0$ that $\beta_{zxx} = \beta_{xxz}$ and $\beta_{zyy} = \beta_{yyz}$ which, clearly, is not the case. We have explicitly checked that this violation is due to the existence of matrix elements of **r** between the states with coinciding energies. When such elements are excluded, Kleinman's symmetry is restored but the point-group symmetry is broken.

Let us proceed to the third-order hyperpolarizability $\gamma_{ijkl}(\omega_1, \omega_2, \omega_3) \equiv \alpha^{(3)}(-(\omega_1 + \omega_2 + \omega_3); \omega_1, \omega_2, \omega_3)$. For different sets of $\{\omega_{1,2,3}\}$, the tensor γ_{ijkl} governs various physical effects. In Table 4 we present the numerical data comprising the following cases. The hyperpolarizability $\gamma(\omega, -\omega, \omega)$ determines such important effects as phase conjugation of light waves, nonlinear corrections to the refraction index and, consequently, self-focusing and optical bistability, optical-frequency Kerr effect, etc. The tensor $\gamma(\omega, 0, \omega)$ governs quasi-SHG, i.e., the generation of the second-harmonic in the presence of a static electric field, and the hyperpolarizability $\gamma(0, \omega, 0)$ is the electro-optical tensor describing the static Kerr effect. For all the cases indicated, the exciting-radiation frequency is that of the Nd:YAG laser, $\hbar\omega = 1.17$ eV or $\lambda = 1.064$ μm. We omit the data for $\gamma(\omega, \omega, \omega)$, since in this case the resulting third-harmonic frequency 3ω is within the region of strong linear absorption of clusters and, therefore, is of less practical interest.

In Table 4 we give values of all nonzero components of the tensor γ and the symmetry-based equalities between these components. For the C_{2v} and T_d clusters, the elements of γ shown in different lines of Table 4 are independent. It can be verified that for the other clusters, there exist linear relations: $\gamma_{xxxx} = 2\gamma_{xxyy} + \gamma_{xyxy}$, and similarly for γ_{yyyy}. The I_h cluster has symmetry with respect to permutation of x, y and z, which implies similar relations also for γ_{zzzz}. The relations mentioned are satisfied by the data

18

of Table 4 with good accuracy.

The numerical results suggest that the magnitude of the third-order hyperpolarizability depends primarily on cluster symmetry and to a lesser degree on the number of atoms. Comparing the data for different clusters, we conclude that the maximum magnitude of γ is predicted for the low-symmetry C_{2v} and C_{3v} clusters. The same clusters possess a strong rectification effect (see Table 3), that suggests an essential role of optical rectification. The latter effect, like charge transfer, brings about the generation of strong static electric fields inside the cluster in response to optical excitation leading to nonlinearity of optical response. Such a mechanism is well known to contribute to large optical nonlinearities of noncentrosymmetric organic molecules, see, e.g., Ref. 29.

In the same manner as above for β, one can estimate the expected magnitude $\gamma \sim \alpha(eL_0/\hbar\Delta\omega)^2 = 6 \times 10^{-33}$ esu, where the same numerical parameters are used. Comparing this estimate to the data of Table 4, we can conclude that for the low-symmetry clusters C_{2v} and C_{3v} the leading elements of γ essentially exceed this estimate, thus revealing high third-order optical responses of these clusters.

Finally, let us discuss the violation of Kleinman's conjecture for the third-order case. The nontrivial (not superceded by the geometrical symmetry) predictions for the considered combinations of frequencies can be obtained for C_{2v}, C_{3v} and D_{5h}, in particular, $\gamma_{zzzx} = \gamma_{zzzz}$, $\gamma_{zzyy} = \gamma_{yyzz}$, etc. These relations are obviously violated (see Table 4). It can be shown that for the weakly nondegenerate hyperpolarizability of the CARS-type $\gamma(\omega, -\omega - \Delta, \omega)$, where $\Gamma \ll \Delta \ll \varepsilon_F/\hbar$, Kleinman's conjecture holds.

19

4. DISCUSSION

The main purpose of this work is to evaluate the electronic contributions to the linear and nonlinear optical properties of small silicon clusters, and also to stimulate experimental studies of small semiconductor clusters with some relevant suggestions. Furthermore, the applicability of the TB method to such calculations can be tested through comparison with (future) experiments and with independent calculations to be done by other methods.

The present semiempirical TB model has been successfully used to predict the structures[17,18] and chemical properties[16] of silicon clusters in the previous works of some of the authors. A semiempirical method with parameters which are fitted to experiments offers an accurate but simple approach to electronic structure for large systems, for which *ab initio* methods are not tractable and may not give sufficient accuracy.[11] Also, we have found the possibility to minimize the geometry without any *a priori* symmetry essential for small silicon clusters.[17]

The applicability of the TB method to describe the optical properties of small silicon clusters is based on the following qualitative arguments. The optical polarizabilities are determined by the electronic structure (positions of the one-electron levels and the matrix elements of dipole transitions between them) and geometry of the clusters. As it was emphasized above, the TB method proved to be successful in the determination of the cluster geometry. On the other hand, its parameters are fitted to correctly reproduce the electronic band structure of bulk silicon. Also, it was shown[17] that they correctly describe the HOMO-LUMO band gap in Si_{10} clusters. Thus, the TB

method is plausible to reproduce positions of one-electron levels. Although the basis set is small, we emphasize that radial forms of the basis functions are not restricted by any explicit dependence. Only the second term in the expression (7) for the dipole moment is estimated using Slater functions, but the results are not sensitive to the specific magnitude of this term: even if this term is completely neglected, the results remain qualitatively the same.

The off-resonance linear polarizability α in Table 2 is determined mainly by the number of atoms N in the cluster and is comparatively insensitive to the structure of the cluster. It obeys the simple estimate $\alpha \simeq N(2.5\text{Å})^3$. In contrast, the absorption spectra of the clusters in Fig. 2 strongly depend on the cluster symmetry. Therefore, experimental study of these spectra can give important structural information, and it may appear to be important in the identification of the cluster structures, which have not been established yet.

The most attractive experimental approach to study optical properties of small clusters would seem to be through the spectroscopy of cluster beams or clusters in low-density vapors. The absorption spectrum of a single cluster, i.e., imaginary part of the polarizability, can be measured in a comparatively simple experiment using photoionization techniques and mass spectrometry. We suggest the following experiment. The probe radiation in the visible or near–IR region from a tunable laser excites clusters which are also subject to high-power IR radiation with longer wavelength. The frequency of the latter should be lower than $\varepsilon_g/\hbar$. Thus, linear absorption of the high-power radiation by the clusters in the ground state is impossible. But once the cluster is excited by the probe radiation, the further step-wise excitation by the high-power radi-

ation is possible and would cause ionization of the cluster with efficiency which may be close to 100 percent. The ionized clusters are detected by a mass spectrometer. In such an experimental arrangement. the amount of ions of a given mass recorded by the mass spectrometer is proportional to the absorption cross-section of the initial (non-ionized) clusters. A good candidate for the light source in these experiments is Nd:YAG laser (λ = 1.064 μm); its fundamental harmonic can serve as the IR radiation, and the second or third harmonic can be used to simultaneously pump the tunable dye laser.

Recently, a similar experiment[30] was performed in which the dissociation cross-sections of small II-V semiconductor clusters have been measured using the photodissociation techniques combined with the mass spectrometry. The information on the absorption spectra was obtained in an indirect way by comparison of the obtained cross-sections to the theory. Note that, in principle, the real part of the linear polarizability of single clusters can also be measured by recording the laser light scattering but, as mentioned above, this quantity is not informative.

Let us discuss the obtained results on nonlinear polarizabilities. The nonlinear optical responses found above govern various coherent (parametric) processes. such as SHG, Pockels effect, phase conjugation, Kerr effect and nonlinear corrections to the refraction index, etc. Such noncoherent nonlinear effects as two- and three-photon absorption, which are determined by the imaginary parts of the third- and fifth-order polarizabilities, will be considered elsewhere. The hyperpolarizabilities should obey symmetry-determined selection rules and relations between their different tensor components. All the symmetry-allowed components of the considered hyperpolarizabilities, together with the corresponding mutual relations, are summarized in Tables 3 and 4.

The symmetry rules and relations are either known from the literature (see. e.g., Ref. 26) or were obtained by symmetry analysis. Since the clusters obtained from the TB calculations obey the corresponding symmetries (see Table 1) with high accuracy and the used diagrammatic formulas are, in principle, exact, the hyperpolarizabilities obtained obey the symmetry-based predictions with negligible errors. This fact has been confirmed by computing all components of the second-order polarizabilities and most of the components of the third-order polarizabilities.

Beside the above discussed geometric symmetries, the hyperpolarizabilities also obey permutation symmetry: any two of the exciting-field frequencies may be exchanged together with the corresponding polarization indices. This symmetry greatly reduces the number of the independent tensor components and is taken into account in Tables 3 and 4. The well-known Kleinman's conjecture also allows the resulting field to be included in the permutation symmetry. For the practically important case of degenerate processes, where the resulting frequency coincides with some of the exciting frequencies, Kleinman's conjecture might allow one to further reduce the amount of independent components. However, we have shown in Sec. 2 that in the degenerate case the Kleinman's conjecture is violated, although it holds for nearly-degenerate cases. when the difference between some of the exciting frequencies and the resulting frequency is much greater than the relaxation rate Γ but much less than the characteristic electron frequency. This result is of general validity. For the clusters considered here it has also been confirmed by numerical results.

The magnitudes of nonlinear responses depend on various qualitative factors among which we should mention the symmetry of clusters, number of atoms N in the cluster,

23

HOMO-LUMO band gap ε_g and delocalization of the cluster orbitals. The explicit dependence of the nth-order polarizability on ε_g for the near-resonant region is given by a simple estimate (see also Sec. 3): $\alpha^{(n)} \sim \alpha(eL_0/(\omega_m - \varepsilon_g))^{(n-1)}$, where ω_m is the largest of the exciting frequencies. Note that $\alpha \propto N$. Thus, the smaller ε_g and the larger n are, the larger is the hyperpolarizability of the cluster. It is intuitively clear that strong delocalization of orbitals may bring about an additional enhancement of optical nonlinearities, the main reason being the increase of the transition dipole matrix elements. This conjecture is often found in the literature.[25,26]

As was already emphasized in Sec. 3, the obtained numerical results in Table 4 show that the symmetry of the clusters, and not the number of atoms ($N = 7 - 10$), is the most essential factor which determines the magnitude of the hyperpolarizabilities. In this respect, the small clusters differ from large clusters and quantum microstructures.

The second-order polarizability β (see Table 3) is the quantity which is known to depend most strongly on the structure of the cluster. The second-order nonlinearity is trivially forbidden for the centrosymmetric I_h cluster, but it is also forbidden for the D_{5h} cluster, which does not have a center of symmetry. The magnitudes found for the leading (largest) elements of β are qualitatively the same for the lower-symmetry C_{2v} and C_{3v} clusters and are considerably less for the higher symmetry T_d cluster. Note that these clusters contain the same number of atoms, $N = 10$. The gap ε_g is substantially smaller for the C_{2v} cluster than for the other clusters (see Table 1). Hence, there should exist a factor which compensates for the effect of ε_g. Such a factor appears to be a small deviation of the C_{2v} cluster from the higher symmetry: this cluster is obtained as the result of the Jahn-Teller distortion of the D_{4d} cluster, for which the second-order

24

nonlinearity is symmetry-forbidden.

The third-order nonlinearity is always allowed, independent of symmetry. But like in the case of second-order nonlinearity, the highest responses are found for the lower-symmetry clusters C_{2v} and C_{3v} (see Table 4). For these clusters, the magnitude of the corresponding hyperpolarizability, $\gamma \sim 10^{-32}$ esu, exceeds by an order of magnitude the maximum estimate (see Sec. 3). It is intuitively clear that the higher the symmetry, the more pronounced may be the delocalization. If so, the effect of delocalization for the considered systems is not substantial. This preliminary conclusion will be tested quantitatively elsewhere. The aggregate of the obtained data suggests that the most essential factor for the third-order nonlinearity in small Si clusters is the symmetry. The enhancement of the nonlinearity in the case of low symmetry may be attributed to optical rectification (charge transfer).

The strong dependence of the polarizabilities on the cluster symmetry is intimately related to the fact that they precisely obey all the symmetry-based selection rules and relations (see above). In particular, for some of the clusters, the second-order polarizabilities simply vanish. For these clusters, the contribution to the third-order polarizability of the static fields, which appear due to the optical rectification effect, is absent. This may partly explain the relatively low third-order polarizabilities of the clusters mentioned. Another example of the direct relation between symmetry and the magnitude of $\alpha^{(2)}$ for the C_{2v} cluster was considered above. These arguments allow us to consider the strong symmetry dependence to be a general feature of small clusters, which is correctly reproduced by the TB model, and it is not a consequence of, e.g., a limited basis set.

25

Since the the optical nonlinearities of the small Si clusters are found to be high, these clusters are promising candidates for making efficient nonlinear optical composite materials. A major problem in this regard is accumulation of the clusters on substrates (surfaces) or in host media where, as the latter, zeolites[8] deserve attention. The second-order nonlinearities may be recorded for aligned clusters on substrates or in crystal matrices, and the third-order for clusters with arbitrary orientation in all media or in dense vapors.

Acknowledgments

APPENDIX: Partial sum rule for dipole transitions

We show here that the first term in right-hand side of Eq. (7) equals zero in a case where overlap of atomic wavefunctions can be neglected, while the multipole interaction may be arbitrarily strong. To begin, we note that the two terms in Eq. (7) can be presented as matrix elements of the two operators $\mathbf{R}$ and $\delta\mathbf{r}$, defined in the shifted atomic basis

$$\mathbf{r} = \mathbf{R} + \delta\mathbf{r}; \quad \langle\mu'b|\mathbf{R}|\mu a\rangle = \delta_{\mu'\mu}\delta_{ab}\mathbf{R}_\mu, \quad \langle\mu'b|\delta\mathbf{r}|a\mu\rangle = \delta_{\mu'\mu}(\mathbf{r})_{ba} \quad . \tag{A.1}$$

From the above definition one can easily see that the operators $\mathbf{R}$ and $\delta\mathbf{r}$ commute mutually and with $\mathbf{r}$ and, consequently, in the coordinate representation both are functions of $\mathbf{r}$. Then we shall follow the familiar derivation of the Thomas-Reiche-Kuhn sum rule. If the Hamiltonian H does not contain a velocity-dependent interaction, we can easily find the double commutator

$$[[H, \mathbf{R}], \mathbf{R}] = -\frac{\hbar^2}{m}(\frac{\partial}{\partial r_i}\mathbf{R})^2 \quad , \tag{A.2}$$

where m is the electron mass. Averaging (A.2) over the ground state $|g\rangle$, we obtain

$$\sum_p (\varepsilon_p - \varepsilon_g)|\mathbf{R}_{pg}|^2 = \frac{\hbar^2}{2m}\sum_{\mu ab}C^*_{p\mu b}C_{g\mu a}\int\varphi^*_b(\mathbf{r})[\frac{\partial}{\partial \mathbf{r}_i}\mathbf{R}(\mathbf{r} - \mathbf{R}_\mu)]\varphi_a(\mathbf{r})d\mathbf{r} \quad . \tag{A.3}$$

The sum rule (A.3) is exact and does not depend on the overlap of the atomic wavefunctions. Now we invoke the no-overlap assumption, whereby the function $\mathbf{R}(\mathbf{r})$ in Eq. (A.1) can easily be found explicitly: $\mathbf{R} = \mathbf{R}_\mu$ when $\mathbf{r}$ belongs to the space occupied by the μ-th atom. It is obvious that in (A.3) the function $\mathbf{R}(\mathbf{r})$ is constant

27

in the region where the atomic wavefunctions $\varphi_{p,q}(\mathbf{r})$ are not zero. It means that the right side of Eq. (A.3) vanishes. Since $\varepsilon_p - \varepsilon_g > 0$, we arrive at the conclusion that the operator $\mathbf{R}(\mathbf{r})$ as a whole is zero. In such a way, if one neglects the overlap of the atomic wavefunctions in a regular way (beginning from determination of the eigenstates), then the C-coefficients in Eq. (7) interfere in such a way that they cancel the first term.

References

1. Q.-L. Zhang, Y. Liu, R. F. Curl, F. K. Tittel and R. E. Smalley, J. Chem. Phys. **88**, 1670 (1988).

2. Y. Liu, Q.-L. Zhang, F. K. Tittel, R. F. Curl and R. E. Smalley, J. Chem. Phys. **85**, 7434 (1986).

3. T. P. Martin and H. Schaber. Z. Phys. **35**, 61 (1979); T. P. Martin and H. Schaber, J. Chem. Phys. **83**, 855 (1985).

4. O. Chesnovsky, S. H. Yang, C. L. Pettiette, M. J. Craycraft, Y. Liu and R. E. Smalley, Chem. Phys. Lett. **138**, 119 (1987); A. Kasuya and Y. Nishina, Z. Phys. D **12**, 493 (1989).

5. Y. Wang, N. Herron, W. Mahler and A. Suna, J. Opt. Soc. Am. B **6**, 808 (1989).

6. Y. Q. Li, C. C. Sung, R. Inguva and C. M. Bowden, J. Opt. Soc. Am. B **6**, 814 (1989); A. E. neeves and M. H. Birnboim, J. Opt. Soc. Am. B **6**, 787 (1989); and D. Stroud and V. E. Wood, J. Opt. Soc. Am. B **6**, 778 (1989).

7. G. T. Boyd, J. Opt. Soc. Am. B **6**, 685 (1989).

8. G. D. Stucky and J. E. MacDougal, Science **47**, 669 (1990).

9. P. Horan and W. Blau, Z. Phys. D **12**, 501 (1989); C. J. Sandroff, J. P. Harbison, R. Ramesh, M. J. Andrejco, M. S. Hegde, D. M. Hwang, C. C. Chang and E. M. Vogel, Science **245**, 391 (1989).

10. S. Schmitt–Rink. D. A. B. Miller. D. S. Chemla. Phys. Rev. B **35**. 8113 (1987): and S. Schmitt–Rink. D. S. Chemla and D. A. B. Miller, Adv. Phys. **38**. 89 (1989).

11. K. Raghavachari and C. M. Rohlfing, J. Chem. Phys. **89**, 2219 (1988).

12. H. Kupka and K. Jug, Chem. Phys. **30**, 23 (1989).

13. P. Ballone, W. Andreoni, R. Car and M. Parrinello, Phys. Rev. Lett. **62**, 292 (1989).

14. J. R. Chelikowsky and J. C. Phillips, Phys. Rev. Lett. **63**, 1653 (1989); J. R. Chelikowsky, J. C. Phillips, M. Kamal and M. Strauss, Phys. Rev. Lett. **62**, 292 (1989).

15. F. Stillinger and T. Weber, Phys. Rev. B **31**, 5262 (1981); J. Tersoff, Phys. Rev. B **37**, 6991 (1988); R. Biswas, C. Z. Wang, C. T. Chan, K. M. Ho and C. M. Soukoulis, Phys. Rev. Lett. **63**, 1491 (1989); A. D. Mistriotis, N. Flytzanis and S. C. Farantos, Phys. Rev. B **39**, 1212 (1989).

16. D. A. Jelski, Z. C. Wu and T. F. George, Chem. Phys. Lett. **150**, 447 (1988); D. A. Jelski, Z. C. Wu and T. F. George, J. Cluster Sci. 1, 143 (1990).

17. T. T. Rantala, D. A. Jelski and T. F. George, J. Cluster Sci., in press.

18. D. Tománek and M. A. Schlüter, Phys. Rev. B **36**, 1208 (1987).

19. K. Laasonen and R. M. Nieminen, J. Phys.: Cond. Matter **2**, 1509 (1990).

30

20. D. J. Chadi. Phys. Rev. B **29**. 785 (1984).

21. J. C. Slater and G. F. Koster Phys. Rev. **94**. 1498 (1954).

22. Z. G. Soos and S. Ramasecha. J. Chem. Phys. **90**, 1067 (1989) [Erratum: J. Chem. Phys. **92**, 5166 (1990)].

23. C. R. Gatz, *Introduction to Quantum Chemistry* (C. E. Merrill Publishing Company, Columbus. Ohio. 1971), p. 180.

24. H. G. Berry, J. Bromander. L. J. Curtis and R. Buchta. Physica Scripta **3**, 125 (1971).

25. S. J. Lalama and A. F. Garito, Phys. Rev. A **20**, 1179 (1979); W. C. Egbert, SPIE Proc. Vol. **824**, 107 (1987); J. W. Wu, J. R. Heflin, R. A. Norwood, K. Y. Wong, O. Zamani-Khamiri, A. F. Garito, P. Kalayanaraman and J. Sounik, J. Opt. Soc. Am. B **6**, 707 (1989).

26. Y. R. Shen, *The Principles of Nonlinear Optics* (Wiley, New York, 1984).

27. T. K. Yee and T. K. Gustafson, Phys. Rev. A **18**, 1597 (1978).

28. D. A. Kleinman, Phys. Rev. **126**, 1977 (1962).

29. G. Marowsky, L. F. Chi, D. Mobius, R. Steinhoff, Y. R. Shen, D. Dorsh and B. Rieger, Chem. Phys. Lett. **147**, 420 (1988).

30. L. K. D. Kolenbrander and M. L. Mandich. J. Chem. Phys. **92**, 4759 (1990).

TABLE 1. Electronic structure data for the Si_7, Si_{10} and Si_{13} clusters. The names are from Ref. 17. E_{coh} is the cohesion energy per atom, and the HOMO–LUMO "band gap" ε_g is given both in the energy and wavelength units.

Name	N	Point group	E_{coh}	ε_g		Coordination		
			(eV/atom)	(eV, μm)		min.	max.	av.
	7	D_{5h}	3.8	1.8	0.69	4	6	4.6
DBTA-I	10	C_{2v}	4.0	1.4	0.87	4	7	5.0
TTP	10	C_{3v}	3.9	2.6	0.48	3	6	4.8
TO	10	T_d	3.6	2.9	0.43	3	6	4.8
	13	I_h	4.4	2.8	0.44	6	12	6.7

TABLE 2. Linear polarizabilities $\alpha_{ij}(\omega)$ of the clusters in units of 10^{-23} cm^3 for different photon energies (in eV) and wavelengths (in μm).

$\hbar\omega$	0.0	0.5	1.0	1.77	1.5	2.33	(eV)
λ				1.064		0.532	(μm)
$\underline{N}$ $\quad$ $\underline{ij}$							
7 $\quad D_{5h}$ $\quad xx,yy$	8	8	8	9	9	15	
zz	6	6	7	7	7	11	
10 $\quad C_{2v}$ $\quad xx$	11	12	14	16	38	3	
yy	10	11	11	12	15	8	
zz	14	14	16	18	43	13	
10 $\quad C_{3v}$ $\quad xx,yy$	12	12	13	13	14	24	
zz	13	13	14	14	15	24	
10 $\quad T_d$ $\quad xx,yy,zz$	13	13	14	14	15	20	
13 $\quad I_h$ $\quad xx,yy,zz$	14	14	14	15	15	17	

TABLE 3. SHG $\beta_{ijk}(\omega,\omega) = \alpha^{(2)}(-2\omega;\omega,\omega)$ and rectification $\beta_{ijk}(-\omega,\omega) = \alpha^{(2)}(0;-\omega,\omega)$ of the clusters C_{2v}, C_{3v} and T_d in units of 10^{-28} esu for different photon energies (in eV).

N	ijk	$\alpha^{(2)}$ $\hbar\omega$	$(-2\omega;\omega,\omega)$					$(0;-\omega,\omega)$			
		0.0	10^{-3}	0.5	1.0	1.17	1.5	0.5	1.0	1.17	1.5
10 C_{2v}	zzz	-2.9	-2.1	-3.9	5.3	3.9	8.8	-3.6	-8.0	-13.8	
	zyy	-1.4	-0.9	-1.6	1.4	-0.3	2.1	-1.7	-3.0	-4.2	
	yyz,yzy	-0.9	-0.9	-1.5	8.1	3.5	6.0	-1.1	-2.0	-2.9	
	zxx	0.2	0.3	0.8	-3.2	-5.1	-2.4	0.2	-0.0	-0.5	
	xxz,xzx	0.4	0.3	0.7	-3.1	6.2	-45.6	0.6	1.6	3.1	
10 C_{3v}	zzz	1.8	1.3	1.6	3.7	7.0	31.2	1.9	2.5	2.8	3.9
	$yxx,xyx,xxy,-yyy$	0.3	0.3	0.3	0.6	1.0	-4.7	0.3	0.3	0.3	0.4
	zxx,zyy	0.8	0.3	0.3	0.4	0.5	-16.0	0.9	1.2	1.4	2.1
	xxz,yyz,xzx,yzy	0.2	0.3	0.4	0.9	1.7	16.5	0.2	0.3	0.3	0.3
10 T_d	$xyz,xzy,$ $yxz,yzx,$ zxy,zyx	-0.5	-0.2	-0.3	-0.5	-0.8	3.4	-0.5	-0.6	-0.7	-0.8

TABLE 4. Hyperpolarizabilities $\gamma_{ijkl}(\omega_1,\omega_2,\omega_3) = \alpha^{(3)}(\Omega;\omega_1,\omega_2,\omega_3)$ in units 10^{-33} esu for the photon energy 1.17 eV (or wavelength 1.064 μm).

$\alpha^{(3)}$	$(-\omega;\omega,-\omega,\omega)$	$(-2\omega;\omega,0,\omega)$	$(-\omega;0,\omega,0)$
7 D_{5h}			
$zzzz$	−0.8	−0.9	−0.5
$xxxx, yyyy$	0.3	−0.0	0.2
$zzxx, zzyy, zz_{\cdots}, yyz$	−0.4	−0.3	−0.2
$xzzx, zyzy$	−0.2	−0.4	−0.2
$xxzz, yyzz, xzzx, yzzy$	−0.2	−0.7	−0.2
$zzxz, yzyz$	−0.2	0.7	0.1
$xxyy, yyxx, xyyx, yxxy$	0.2	−0.0	0.0
$xyxy, yxyx$	−0.0	0.0	0.1

35

TABLE 4 (continued)

$$\alpha^{(3)} \quad (-\omega:\omega.-\omega.\omega) \quad (-2\omega:\omega.0.\omega) \quad (-\omega:0.\omega.0)$$

10 C_{2v}

	$(-\omega:\omega.-\omega.\omega)$	$(-2\omega:\omega.0.\omega)$	$(-\omega:0.\omega.0)$
$zzzz$	−20.9	−2.1	15.2
$xxxx$	−21.7	2.1	−3.4
$yyyy$	−0.3	−0.8	2.0
$zzxx.zxxz$	−7.8	1.5	−3.0
$zxzx$	3.4	0.7	3.2
$zzyy,zyyz$	−3.4	−0.8	4.9
$zyzy$	−1.6	2.4	4.8
$yyzz,yzzy$	−3.6	−0.4	4.9
$yzyz$	−1.6	−1.1	3.6
$yyxx,yxxy$	−2.8	0.2	−1.3
$xyxy$	3.0	−1.2	1.0
$xxzz,xzzx$	−15.6	0.5	−3.0
$xzxz$	3.4	1.1	−0.1
$xxyy,xyyx$	−2.6	−0.8	−1.3
$yxyx$	3.0	−1.5	2.3

TABLE 4 (continued)

$\alpha^{(3)}$	$(-\omega:\omega,-\omega,\omega)$	$(-2\omega:\omega,0,\omega)$	$(-\omega:0,\omega,0)$
10 C_{3v}			
$zzzz$	9.3	20.9	3.4
$xxxx, yyyy$	0.1	3.4	−0.0
$zyyy, -zyxx, -zxyx, -zxxy$	−0.1	−0.5	0.0
$yzyy, -yzxx, -xzyx, -xzxy,$			
$yyyz, -yxxz, -xxyz, -xyxz$	−0.3	−0.9	−0.1
$yyzy, -yxzx, -xyzx, -xxzy$	−0.5	−1.3	−0.6
$zzxx, zzyy, zxxz, zyyz$	0.6	0.5	0.0
$zxzx, zyzy$	0.1	−0.0	0.2
$xxzz, yyzz, xzzx, yzzy$	0.3	1.1	1.8
$xzxz, yzyz$	−0.0	−0.5	2.5
$xxyy, yyxx, xyyx, yxxx$	0.1	1.3	0.1
$xyxy, yxyx$	−0.2	0.9	−0.2

TABLE 4 (continued)

	$\alpha^{(3)}$	$(-\omega:\omega,-\omega,\omega)$	$(-2\omega:\omega,0,\omega)$	$(-\omega:0,\omega,0)$
10 T_d				
$xxxx, yyyy, zzzz$		0.8	1.7	0.6
$xxyy, xxzz, yyxx, yyzz,$				
$zzxx, zzyy, xyyx, xzzx,$				
$yxxy, yzzy, zxxz, zyyz$		0.4	0.4	0.2
$xyxy, xzxz, yxyx, yzyz,$				
$zxzx, zyzy$		0.2	−0.1	0.1

TABLE 4 (continued)

	$\alpha^{(3)}$	$(-\omega:\omega.-\omega.\omega)$	$(-2\omega:\omega.0.\omega)$	$(-\omega:0.\omega.0)$
13 I_h				
$xxxx, yyyy, zzzz$		3.7	0.8	1.7
$xxyy, xxzz, yyxx, yyzz,$				
$zzxx, zzyy, xyyx, xzzx,$				
$yxxy, yzzy, zxxz, zyyz$		2.0	0.3	0.3
$xyxy, xzxz, yxyx, yzyz,$				
$zxzx, zyzy$		-0.2	0.2	1.2

FIGURE CAPTIONS

1. Structures of the clusters: (a) Si_7 (D_{5h}), (b) Si_{10}:DBTA-I (C_{2v}), (c) Si_{10}:TTP (C_{3v}), (d) Si_{10}:TO (T_d) and (e) Si_{13} (I_h).

2. Absorption cross-sections of silicon clusters in the same order as in Fig. 1.

Fig. 1(a)

Fig. 1(3)
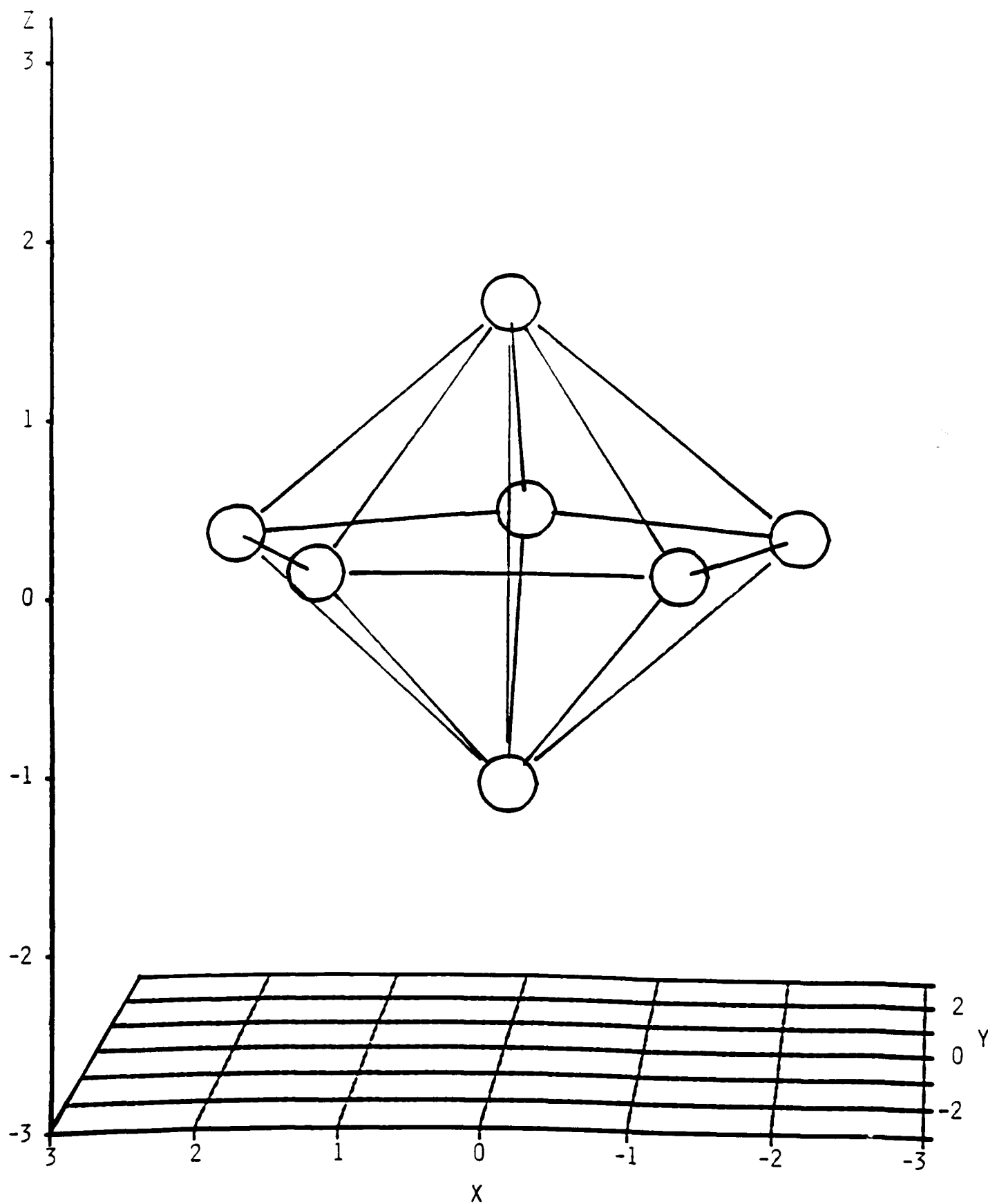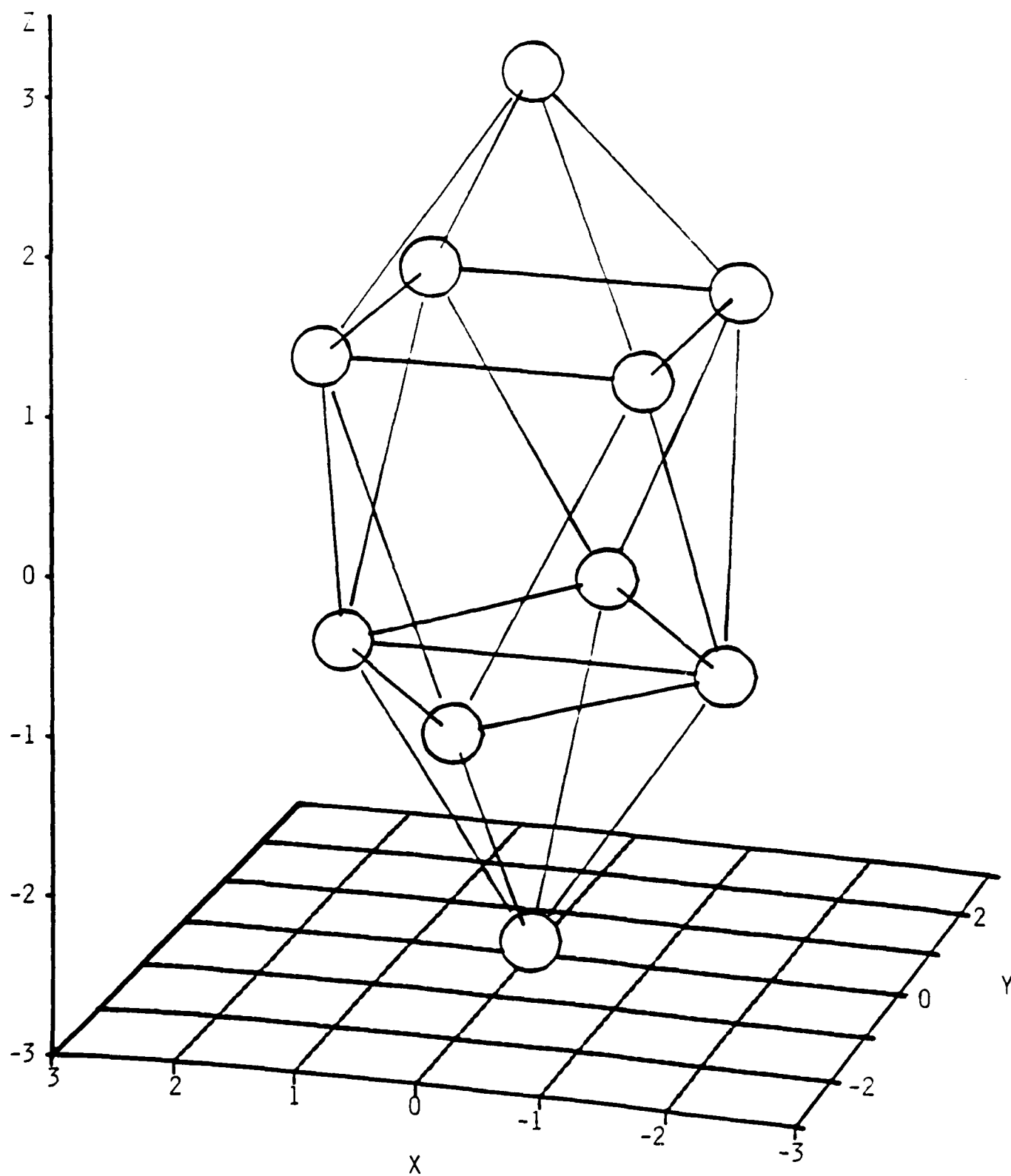
Fig. 1(c)
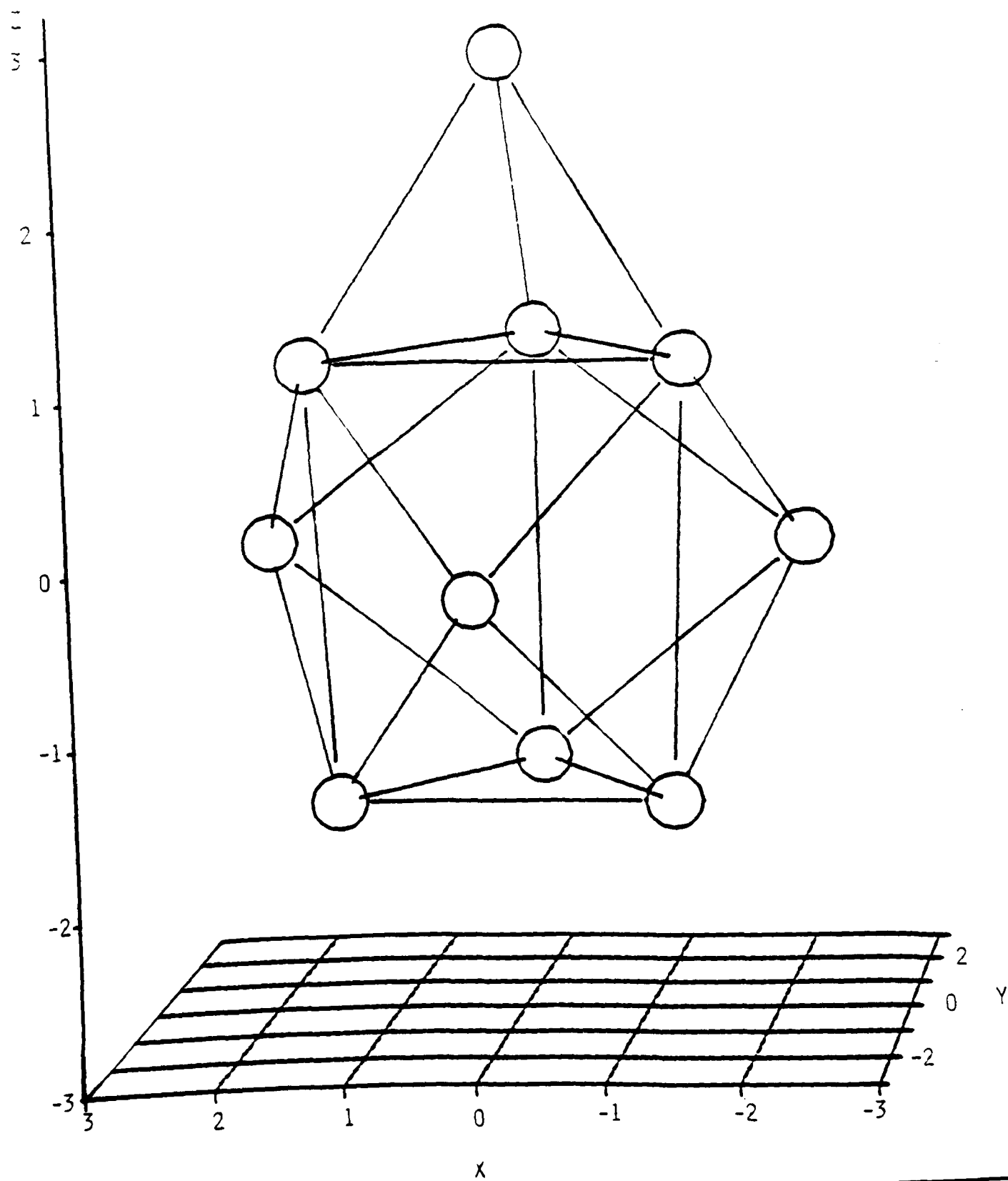
Fig. 11d.

Fig 1(e)

Fig. 2(a)

Fig. 2(2)

Fig. 2(c)

The y-axis is labeled "X-section (10^{-14} cm^2)" with values 0.0, 2.0, 4.0. The x-axis is labeled "Photon energy (eV)" with values 0.0, 2.0, 4.0.

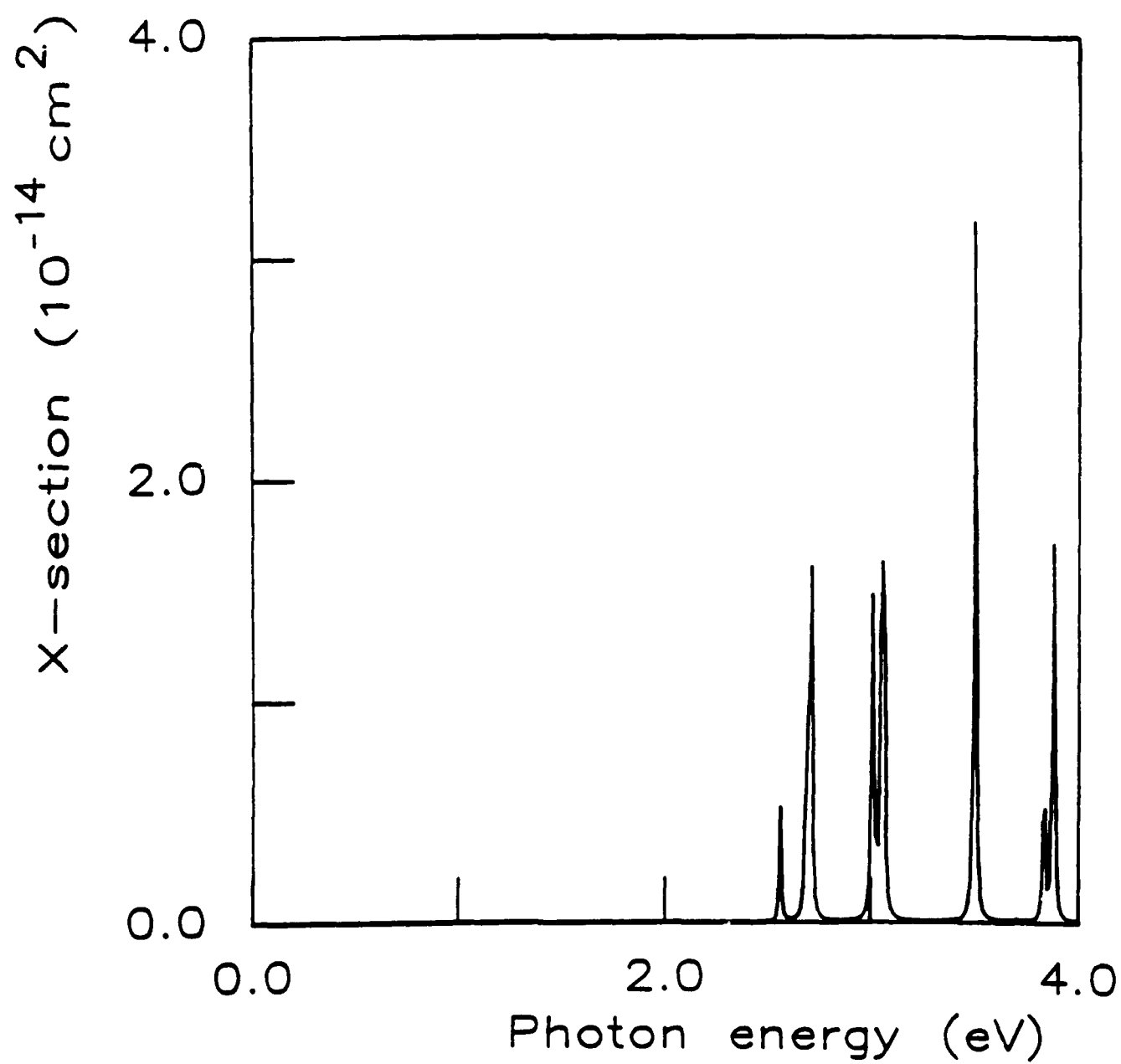Fig. 2(d
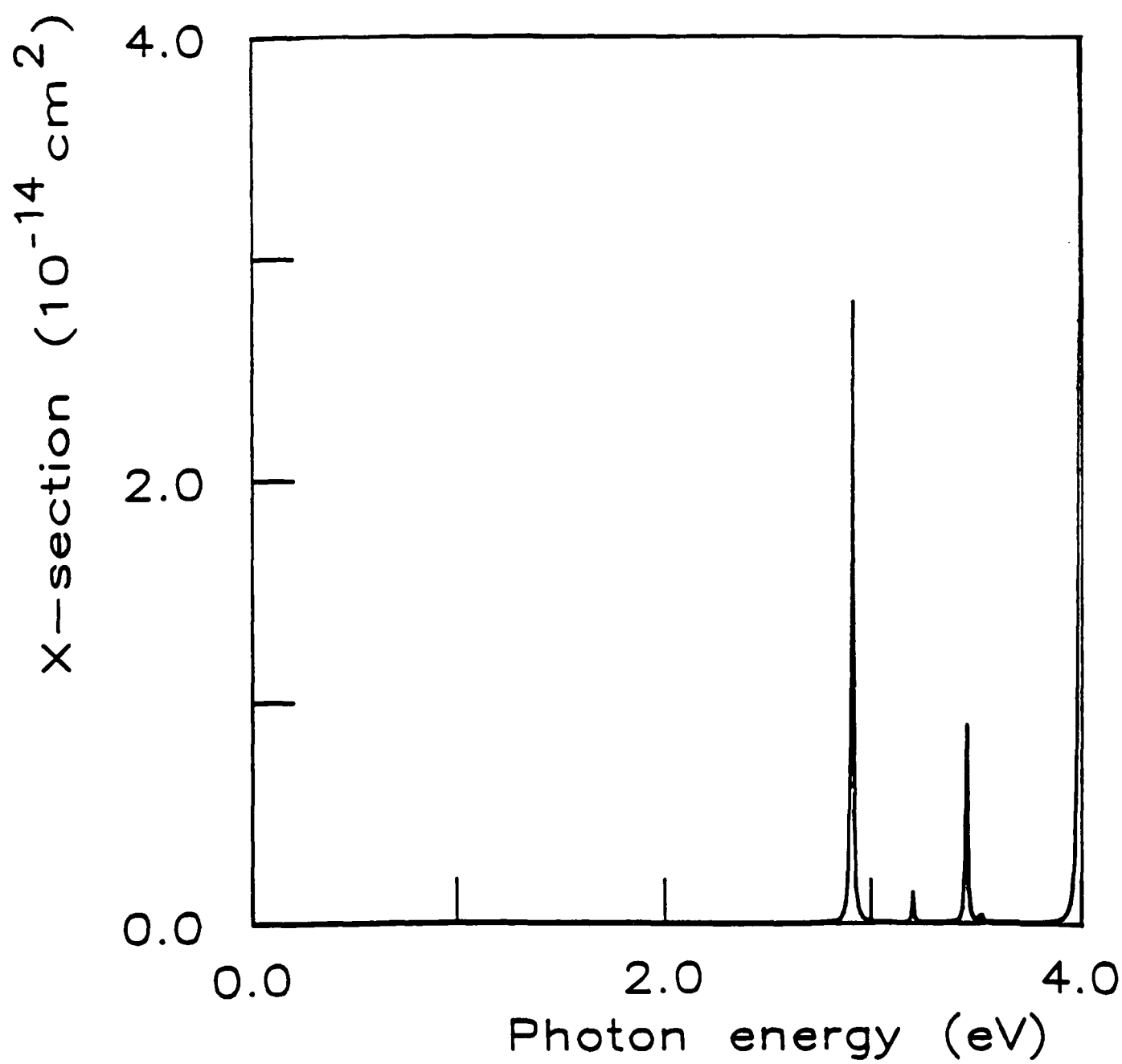
X-section ($10^{-14}\,cm^2$) vs Photon energy (eV)
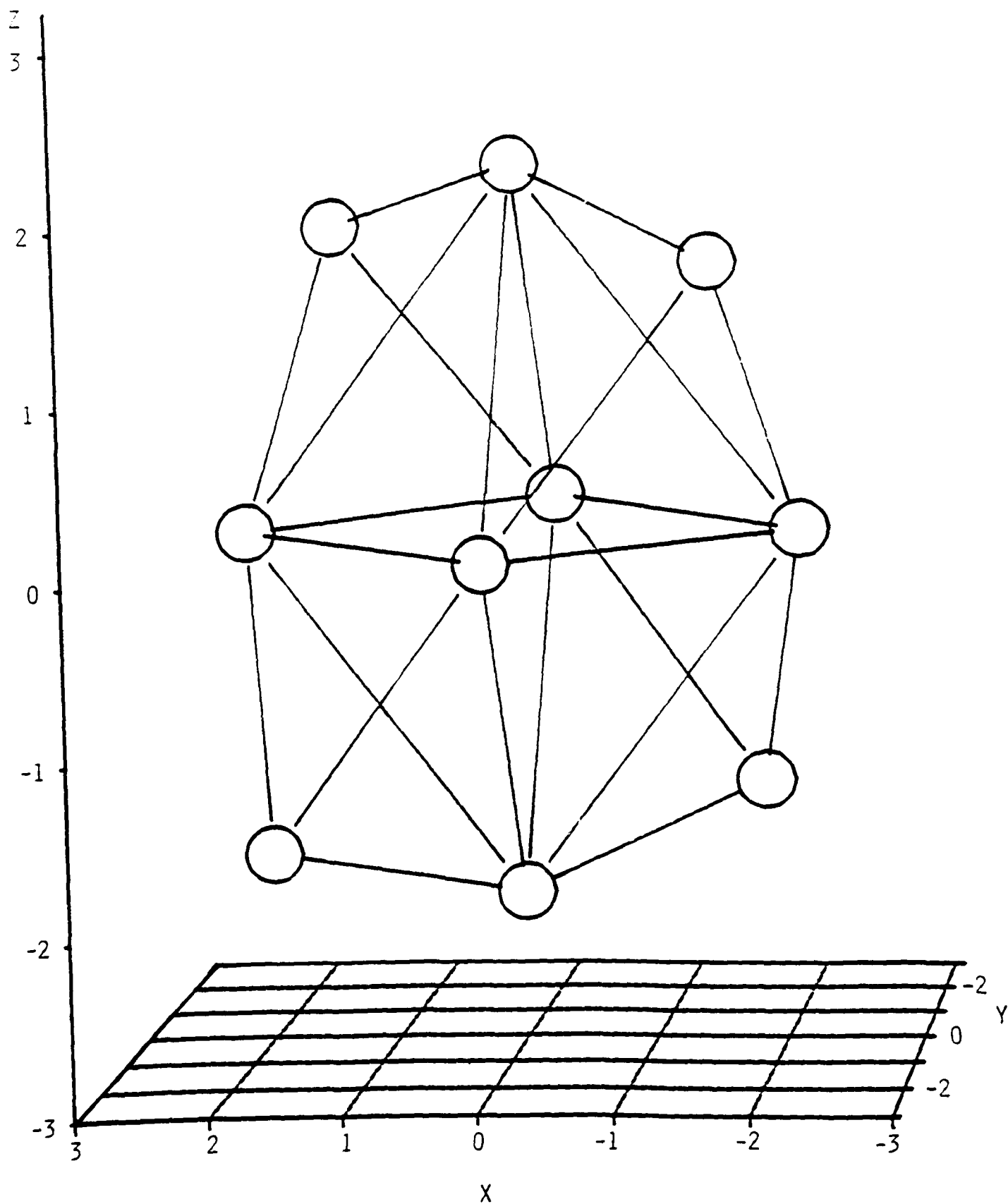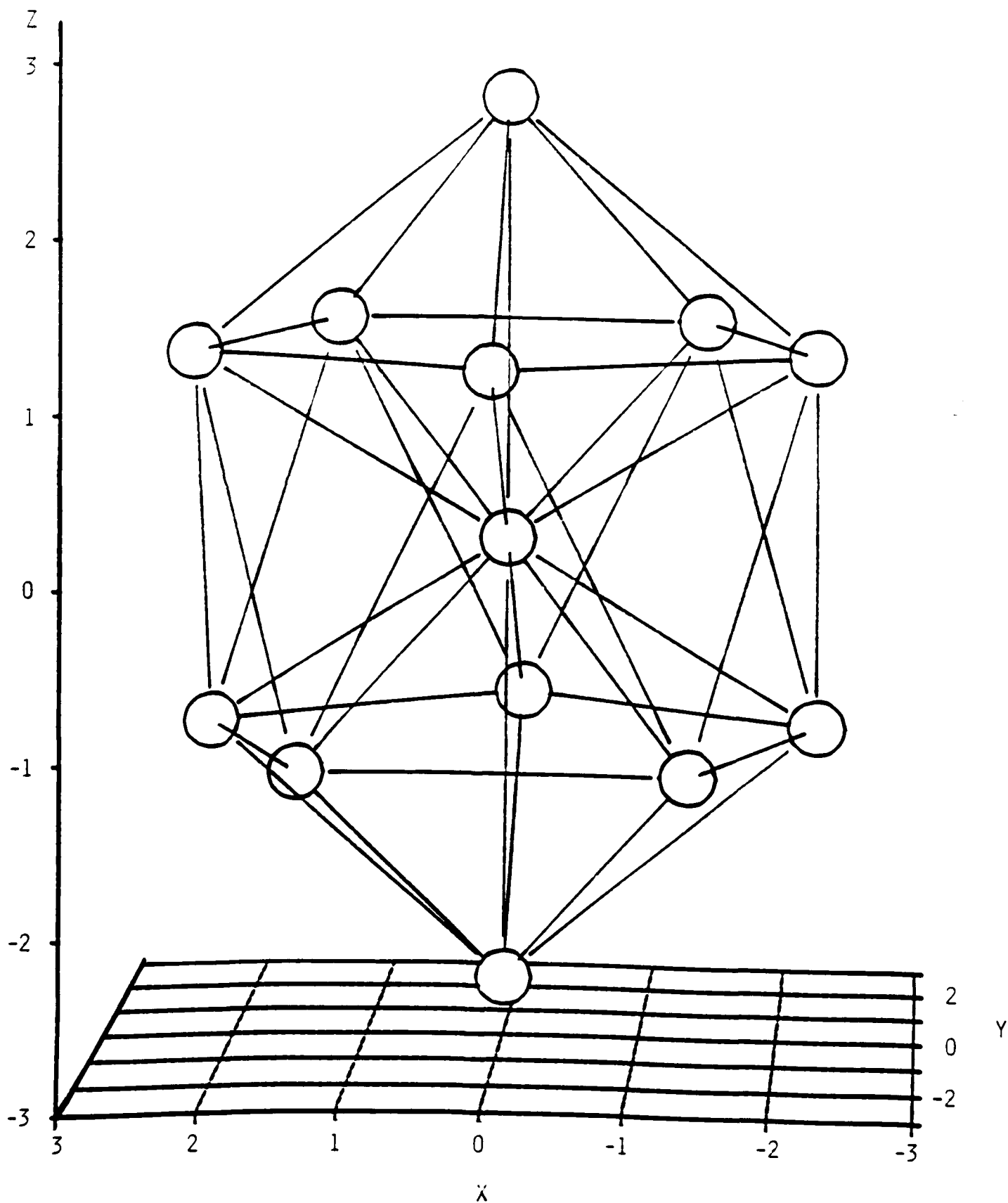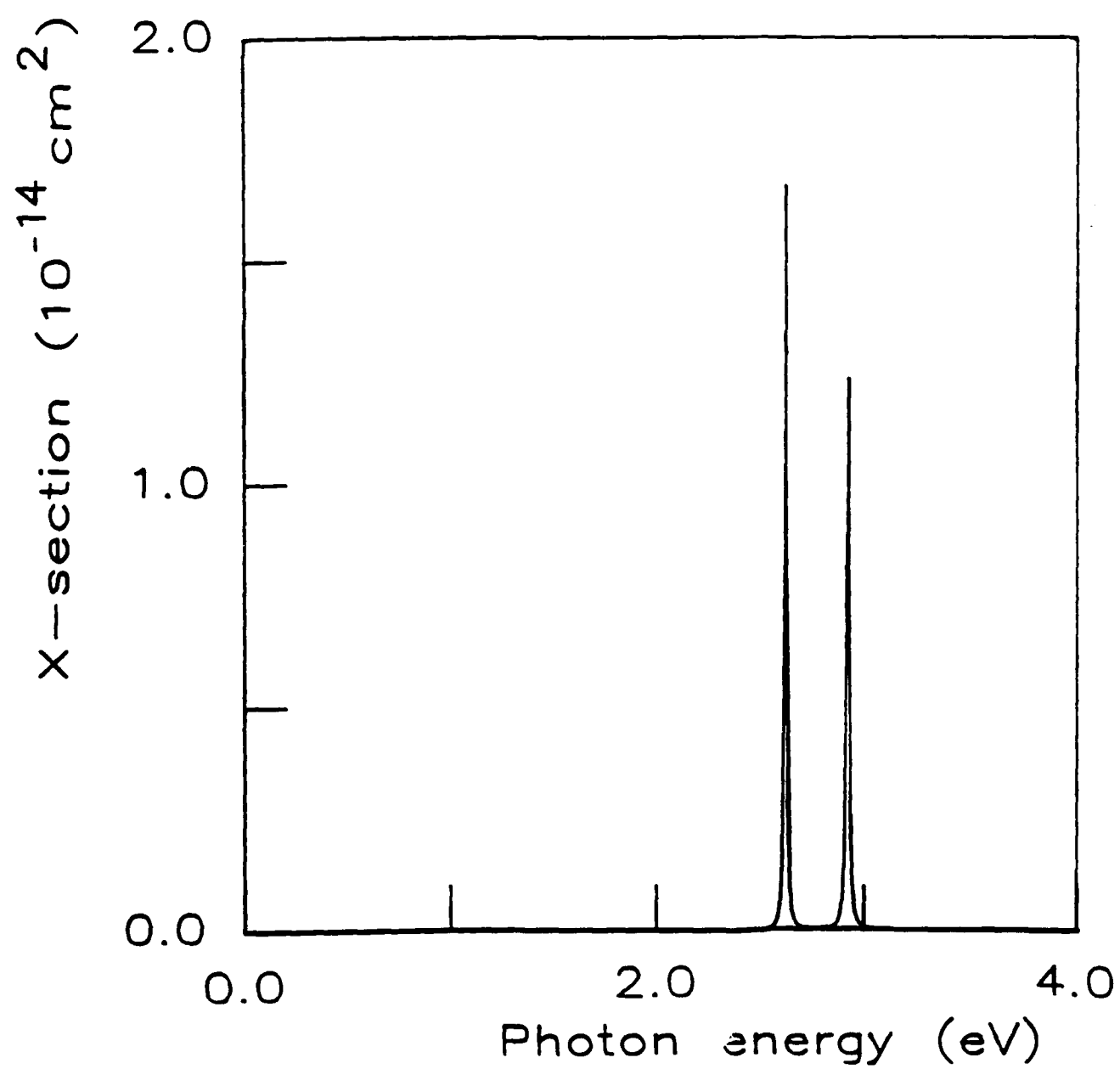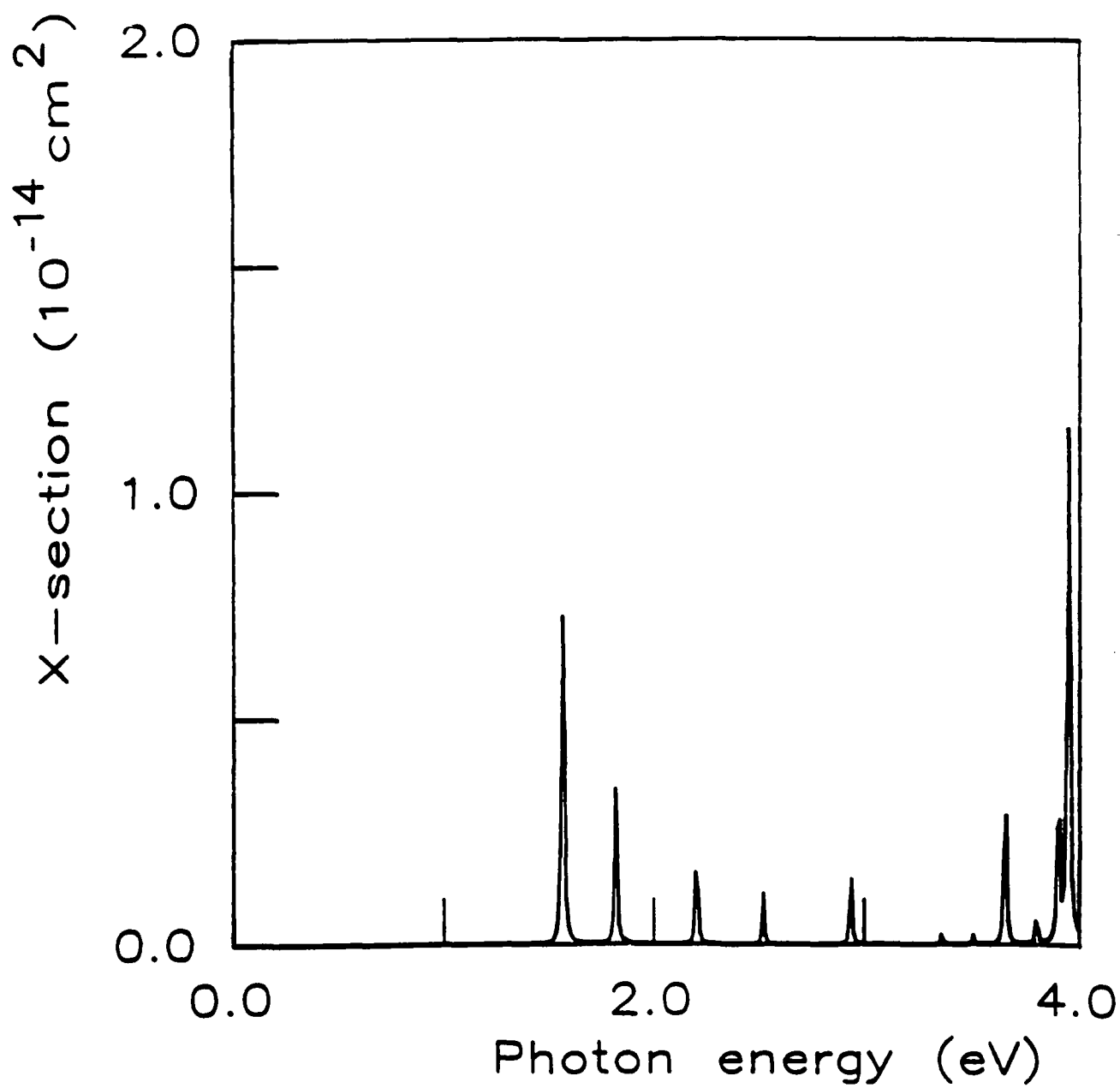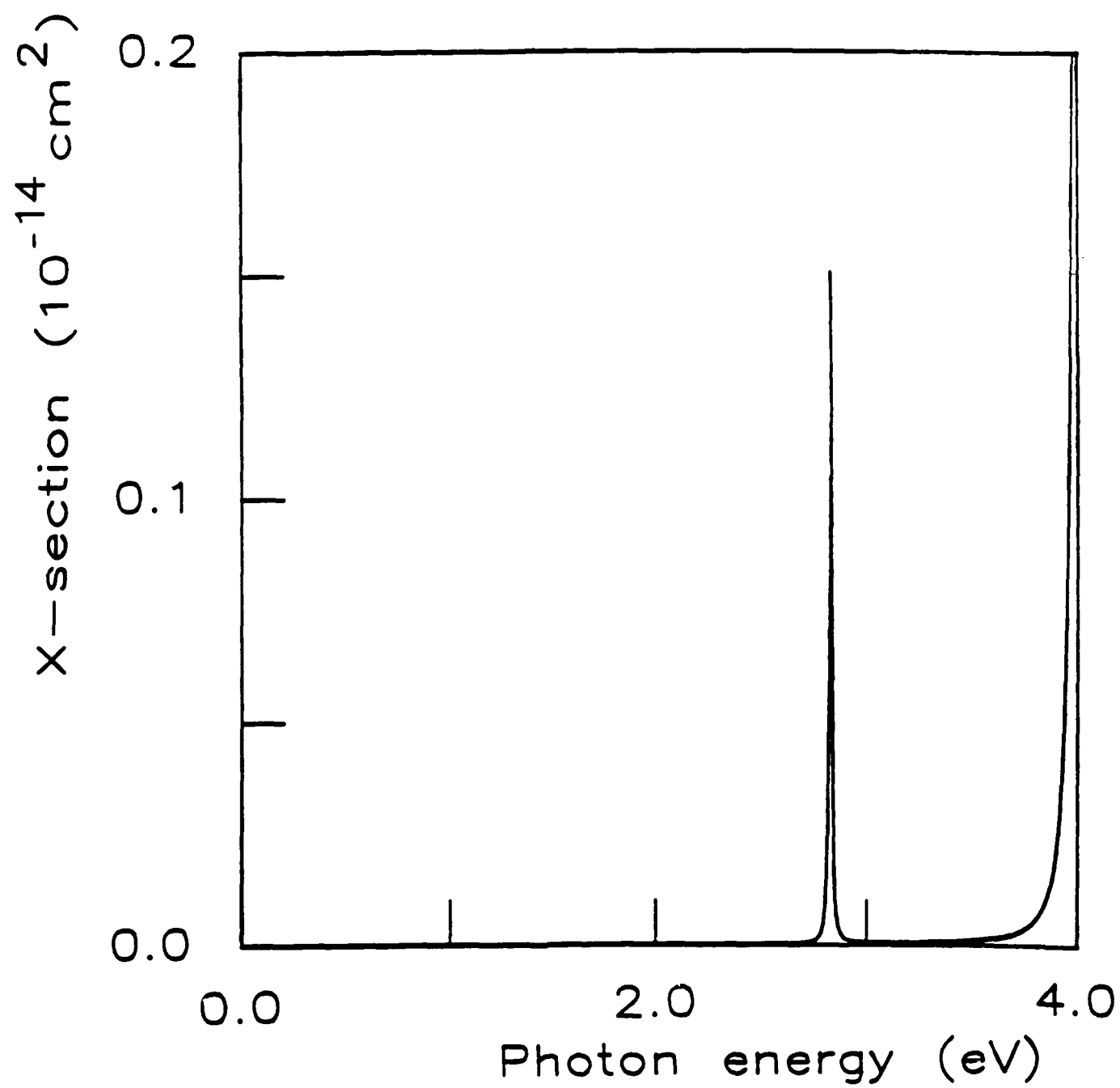
Fig. 2(e)

TECHNICAL REPORT DISTRIBUTION LIST - GENERAL

Office of Naval Research   (2)
Chemistry Division, Code 1113
800 North Quincy Street
Arlington, Virginia 22217-5000

Dr. Robert Green, Director   (1)
Chemistry Division, Code 385
Naval Weapons Center
China Lake, CA 93555-6001

Commanding Officer   (1)
Naval Weapons Support Center
Dr. Bernard E. Douda
Crane, Indiana 47522-5050

Chief of Naval Research   (1)
Special Assistant for Marine
   Corps Matters
Code 00MC
800 North Quincy Street
Arlington, VA 22217-5000

Dr. Richard W. Drisko   (1)
Naval Civil Engineering
 Laboratory
Code L52
Port Hueneme, CA   93043

Dr. Bernadette Eichinger   (1)
Naval Ship Systems Engineering
   Station
Code 053
Philadelphia Naval Base
Philadelphia, PA 19112

David Taylor Research Center (1)
Dr. Eugene C. Fischer
Annapolis, MD 21402-5067

Dr. Sachio Yamamoto   (1)
Naval Ocean Systems Center
Code 52
San Diego, CA 92152-5000

Dr. James S. Murday   (1)
Chemistry Division, Code 6100
Naval Research Laboratory
Washington, D.C. 20375-5000

Dr. Harold H. Singerman   (1)
David Taylor Research Center
Code 283
Annapolis, MD 21402-5067

Dr. David L. Nelson   (1)
Chemistry Division
Office of Naval Research
800 North Quincy Street
Arlington, Virginia 22217

Defense Technical Information Center   (2)
Building 5, Cameron Station
Alexandria, VA 22314

Professor John Baldeschwieler
Department of Chemistry
California Inst. of Technology
Pasadena, CA 91125

Professor Steven George
Department of Chemistry
Stanford University
Stanford, CA 94305

Professor Paul Barbara
Department of Chemistry
University of Minnesota
Minneapolis, MN 55455-0431

Professor Tom George
Dept. of Chemistry & Physics
State University of New York
Buffalo, NY 14260

Dr. Duncan Brown
Advanced Technology Materials
520-B Danury Rd.
New Milford, CT 06776

Dr. Robert Hamers
IBM T.J. Watson Research Center
P.O. Box 218
Yorktown Heights, NY 10598

Professor Stanley Bruckenstein
Department of Chemistry
State University of New York
Buffalo, NY 14214

Professor Paul Hansma
Department of Physics
University of California
Santa Barbara, CA 93106

Professor Carolyn Cassady
Department of Chemistry
Miami University
Oxford, OH 45056

Professor Charles Harris
Department of Chemistry
University of California
Berkeley, CA 94720

Professor R.P.H. Chang
Dept. Matls. Sci. & Engineering
Northwestern University
Evanston, IL 60208

Professor John Hemminger
Department of Chemistry
University of California
Irvine, CA 92717

Professor Frank DiSalvo
Department of Chemistry
Cornell University
Ithaca, NY 14853

Professor Roald Hoffmann
Department of Chemistry
Cornell University
Ithaca, NY 14853

Dr. James Duncan
Federal Systems Division
Eastman Kodak Company
Rochester, NY 14650-2156

Professor Leonard Interrante
Department of Chemistry
Rensselaer Polytechnic Institute
Troy, NY 12181

Professor Arthur Ellis
Department of Chemistry
University of Wisconsin
Madison, WI 53706

Professor Eugene Irene
Department of Chemistry
University of North Carolina
Chapel Hill, NC 27514

Professor Mustafa El-Sayed
Department of Chemistry
University of California
Los Angeles, CA 90024

Dr. Sylvia Johnson
SRI International
333 Ravenswood Avenue
Menlo Park, CA 94025

Professor John Eyler
Department of Chemistry
University of Florida
Gainesville, FL 32611

Dr. Zakya Kafafi
Code 6551
Naval Research Laboratory
Washington, DC 20375-5000

Professor James Garvey
Department of Chemistry
State University of New York
Buffalo, NY 14214

Professor Larry Kesmodel
Department of Physics
Indiana University
Bloomington, IN 47403

Professor Max Lagally
Dept. Metal. & Min. Engineering
University of Wisconsin
Madison, WI 53706

Dr. Stephen Lieberman
Code 522
Naval Ocean Systems Center
San Diego, CA 92152

Professor M.C. Lin
Department of Chemistry
Emory University
Atlanta, GA 30322

Professor Fred McLafferty
Department of Chemistry
Cornell University
Ithaca, NY 14853-1301

Professor Horia Metiu
Department of Chemistry
University of California
Santa Barbara, CA 93106

Professor Larry Miller
Department of Chemistry
University of Minnesota
Minneapolis. MN 55455-0431

Professor George Morrison
Department of Chemistry
Cornell University
Ithaca, NY 14853

Professor Daniel Neumark
Department of Chemistry
University of California
Berkeley, CA 94720

Professor David Ramaker
Department of Chemistry
George Washington University
Washington, DC 20052

Dr. Gary Rubloff
IBM T.J. Watson Research Center
P.O. Box 218
Yorktown Heights, NY 10598

Professor Richard Smalley
Department of Chemistry
Rice University
P.O. Box 1892
Houston, TX 77251

Professor Gerald Stringfellow
Dept. of Matls. Sci. & Engineering
University of Utah
Salt Lake City, UT 84112

Professor Galen Stucky
Department of Chemistry
University of California
Santa Barbara, CA 93106

Professor H. Tachikawa
Department of Chemistry
Jackson State University
Jackson, MI 39217-0510

Professor William Unertl
Lab. for Surface Sci. & Technology
University of Maine
Orono, ME 04469

Dr. Terrell Vanderah
Code 3854
Naval Weapons Center
China Lake, CA 93555

Professor John Weaver
Dept. of Chem. & Mat. Sciences
University of Minnesota
Minneapolis, MN 55455

Professor Brad Weiner
Department of Chemistry
University of Puerto Rico
Rio Piedras, Puerto Rico 00931

Professor Robert Whetten
Department of Chemistry
University of California
Los Angeles, CA 90024

Professor R. Stanley Williams
Department of Chemistry
University of California
Los Angeles, CA 90024

Professor Nicholas Winograd
Department of Chemistry
Pennsylvania State University
University Park, PA 16802

Professor Aaron Wold
Department of Chemistry
Brown University
Providence, RI 02912

Professor Vicki Wysocki
Department of Chemistry
Virginia Commonwealth University
Richmond, VA 23284-2006

Professor John Yates
Department of Chemistry
University of Pittsburgh
Pittsburgh, PA 15260